

Exploring the spatiotemporal patterns of theta-band activity during rapid-eye movement sleep:
a magnetoencephalography analysis

Vasiliki Provias

A Thesis in
The Department
of
Psychology

Presented in partial fulfilment of the
requirements for the degree of
Master of Arts (Experimental Psychology)
at Concordia University, Montréal, Québec

August 2024

© Vasiliki Provias

CONCORDIA UNIVERSITY

School of Graduate Studies

This is to certify that the thesis

Prepared by: Vasiliki Provias

Entitled: Exploring the spatiotemporal patterns of theta-band activity during rapid-eye movement sleep: a magnetoencephalography analysis

and submitted in partial fulfilment of the requirements for the degree of

Master of Arts (Experimental Psychology)

complies with the regulations of the University and meets the accepted standards with respect to originality and quality.

Signed by the final Examining Committee:

_____ Chair: Karen Li

_____ Examiner: Thien Thanh Dang-Vu

_____ Examiner: Christopher Steele

_____ Supervisor: Emily BJ Coffey

Approved by _____ (Karen Li)
(Chair of Department or Graduate Program Director)

Date: 25th of July 2024 _____ (Pascale Sicotte)

Abstract

Exploring the spatiotemporal patterns of theta-band activity during REM sleep: a MEG analysis

Vasiliki Provias

Theta oscillations (4-8 Hz) are a prominent electrophysiological feature of rapid-eye movement (REM) sleep. Theta activity during REM sleep has been linked to memory consolidation; however, the role of cortical theta oscillations in this process remains unclear. Interestingly, theta rhythms are not exclusive to REM sleep but also appear in frontal regions during resting wakefulness and working memory tasks. To advance our understanding of human REM sleep and the mechanisms that support memory processing, a spatially resolved, whole-brain characterisation of REM oscillatory activity is essential. Magnetoencephalography (MEG) offers high temporal and spatial resolution, making it ideal for examining the topographic distribution of theta oscillations in REM sleep. In this study, we recorded electroencephalography (EEG)/MEG data during overnight sleep in 10 healthy subjects. We also analysed a separate MEG/EEG data of 17 healthy subjects who performed a working memory task. Our aims were to characterise the spatio-temporal patterns of theta-band activity during REM sleep by 1) distinguishing theta from the overlapping alpha (8-12 Hz) network, 2) comparing REM and non-rapid-eye movement (NREM) sleep oscillatory activity, and 3) evaluating similarities between REM and working memory task theta patterns. Our results show theta activity in frontal mid-line regions is best observed within a focused 5-7 Hz range, separating it from occipital alpha activity. Theta-band activity was greater in REM sleep compared to NREM in frontal-central, parietal, temporal, and subcortical regions. Theta topographies during the working memory task correlated positively with phasic REM sleep. These results enhance our understanding of REM sleep physiology and suggest future research targets for learning and memory roles. Current research has primarily focused on theta activity in isolated regions or during specific states, leaving gaps in our understanding of its whole-brain distribution and substate differentiation.

Keywords: theta; REM sleep; MEG; memory consolidation; working memory

Acknowledgments

I would like to express my deepest gratitude to several individuals who have supported and contributed to this work:

First and foremost, I am profoundly grateful to my supervisor, Dr. Emily Coffey, whose guidance, expertise, and unwavering support have been instrumental in shaping and advancing this research. Thank you for beginning a significant portion of this study in 2018 and laying the foundation for what it has become today. Your insightful feedback and mentorship have been invaluable.

Special thanks to Lea Himmer and Lore Wagner for their dedication in collecting the sleep data. Your hard work and meticulous attention to detail have greatly contributed to the quality of this study.

I am also grateful to Alberto Romero Ara and Hugo Jourde for their assistance in building the linear mixed-effects models for our analyses. Your expertise in statistical modeling has been essential to this research.

To Philippe Albouy, thank you for generously allowing us to use your working memory dataset. Your contribution has significantly expanded the scope and depth of this research.

I would also like to extend my heartfelt thanks to everyone in Dr. Coffey's lab. The welcoming and collaborative environment made a significant difference in this journey. Your readiness to help and your supportive nature created an ideal setting for research and personal growth.

Contribution of Authors

Provias, V., Schönauer, M., Gais, S., Albouy, P., Born, J., Bergmann, T.O., & Coffey, E.B.J.

Vasiliki Provias: Conceptualisation; Methodology; Formal analysis; Software; Visualisation; Writing—original draft; Writing—review and editing. **Monika Schönauer:** Conceptualisation; Writing—review and editing. **Steffan Gais:** Data collection; Conceptualisation; Resources; Funding acquisition; Writing—review and editing. **Jan Born:** Conceptualisation; Resources; Funding acquisition; Supervision; Writing—review and editing. **Til O. Bergmann:** Conceptualisation; Methodology; Supervision; Writing—review and editing. **Emily B.J. Coffey:** Conceptualisation; Resources; Methodology; Formal analysis; Data curation; Writing—original draft; Writing—review and editing; Supervision; Project administration; Funding acquisition.

document:

Table of Contents

Abstract	iii
Acknowledgements	iv
Contribution of authors	v
List of figures	vi
List of tables	vii
List of abbreviations	viii
Introduction	1
Methods	6
Results	14
Discussion	20
References	29
Supplementary	41

List of Figures

Figure 1	16
Figure 2	17
Figure 3	19
Figure 4	20

List of Tables

Table 1	14
---------------	----

List of Abbreviations

AAL Automated Anatomical Labeling Atlas

AICHA Atlas of Intrinsic Connectivity of Homotopic Areas Atlas

ACC Anterior Cingulate Cortex

dIPFC Dorsolateral Prefrontal Cortex

mPFC Medial Prefrontal Cortex

EEG Electroencephalography

EMG Electromyography

EOG Electrooculography

fMRI Functional Magnetic Resonance Imaging

IRASA Irregular Resampling Auto-Spectral Analysis

LGN Lateral Geniculate Nucleus

LME Linear Mixed Effects Modelling

NREM Non-Rapid Eye Movement

PET Positron Emission Tomography

PPN Pedunculopontine Nucleus

REM Rapid-Eye Movement

TMS Transcranial Magnetic Stimulation

1 Introduction

Sleep plays an important role in memory consolidation — the process of transforming initially fragile memory traces into strong and stable representations (Diekelmann & Born, 2010). While there is substantial evidence supporting the role of non-rapid-eye movement (NREM) sleep in memory consolidation, the specific contribution of rapid-eye movement (REM) sleep is less well-understood (Ackermann & Rasch, 2014; Brodt et al., 2023; Klinzing, Niethard, & Born, 2019; Luthi & Fernandez, 2020). Research on the direct contribution of REM sleep to memory consolidation has yielded inconsistent results. While studies suggest that REM sleep promotes the consolidation of emotional and procedural memories, including creative problem-solving (Wagner et al., 2001; Hu et al., 2006; Nishida et al., 2009; Groch et al., 2013; Gujar et al., 2011; Lewis et al., 2018), other studies do not support these findings (Baran et al., 2011; Vertes & Eastman, 2000), leading some researchers to propose that REM sleep may support memory consolidation only indirectly through mechanisms such as altering neural firing patterns and synaptic rescaling (Grosmark et al., 2012; Tononi & Cirelli, 2014). However, the extent to which REM sleep aids in memory consolidation and the specific neural mechanisms underlying this process in humans remain unclear.

Insights into REM sleep's more direct cognitive roles may be gained by examining its physiological underpinnings. Neuroimaging modalities such as positron emission tomography (PET) and functional magnetic resonance imaging (fMRI) have contributed to identifying brain regions and networks involved in REM sleep (Braun et al., 1997, 1998; Corsi-Cabrera et al., 2008; Hong et al., 1995; Ioannides et al., 2004; Maquet et al., 1996, 2000, 2005; Madsen & Vorstrup, 1991; Miyauchi et al., 2008; Nofzinger et al., 1997; Peigneux et al., 2001; Wehrle et al., 2005, 2007). PET studies reveal increased regional cerebral blood flow (rCBF) in both cortical and subcortical regions compared to NREM sleep (Braun et al., 1997; Maquet et al., 2005). Specifically, increased rCBF has been observed in cortical regions such as the medial prefrontal cortex (mPFC), inferior frontal gyrus, anterior cingulate cortex (ACC), superior parietal cortex, precuneus, and unimodal sensory areas, as well as in subcortical regions including the amygdala, brainstem, thalamus, basal ganglia, paralimbic-limbic areas, and the lateral geniculate bodies (Braun et al., 1997; Maquet et al., 2005). Many of the

same regions have also been observed using fMRI, which indexes regional changes in blood oxygenation. For example, Wehrle et al. (2005, 2007) reported activity in REM within the thalamus, amygdala, entorhinal cortex, and anterior cingulate, as well as the visual cortex and putamen. Particularly when analyses are time-locked to eye movements, visual system regions such as the pontine tegmentum, ventroposterior thalamus, and primary visual cortex are strongly active (Miyachi et al., 2008).

While PET and fMRI studies provide essential spatial information about brain activity, they do not provide information concerning the frequency-specificity of REM-related activity; for this purpose, EEG, MEG, and intracranial recordings are useful. EEG studies of REM sleep indicate that brain activity exhibits low-amplitude, mixed-frequency patterns closely resembling wakefulness (Brodt et al., 2023; Rasch & Born, 2013); this similarity led to REM sleep being termed 'paradoxical sleep', highlighting the seemingly contradictory state of an active mind within a sleeping body (Jouvet, 1965). Several frequency bands are observed to be amplified during REM sleep, including delta (1-4 Hz), theta (4-8 Hz), alpha (8-12 Hz), beta (18-30 Hz), and gamma (30-100 Hz) - noting that these frequency band divisions are not universally agreed upon and activity may be overlapping (Cantero et al., 2003, 2004; Cape et al., 2000; Montgomery et al., 2008; Nishida et al., 2009; Scheffzük et al., 2011; Simor et al., 2016, 2020, 2021; Vijayan et al., 2017).

More focused comparisons between brain states show a pattern of frontal activity in the lower of these frequency ranges that is elevated in REM sleep as compared with the wake state, and as compared to the NREM sleep stages (Simor et al., 2019; Achermann et al., 2016; Baird et al., 2018). Several studies have used source reconstruction methods to map activity that is recorded at the scalp back onto the brain, a technique which offers additional spatial information. For example, Baird et al. (2018) report elevated activity between 1-7 Hz in REM that was observed at the frontal midline in the sensor space (scalp) analysis and was localised to dorsal frontal regions in the brain. Magnetoencephalography is preferable for source reconstruction as unlike electrical fields, magnetic fields are not distorted by tissue interfaces through which they pass (Baillet et al., 2017). Although MEG can be used to look at the whole brain including deeper sources (Coffey et al., 2021); the few extent MEG studies

of REM sleep have tended to focus only on the cortex and have noted activity in the (left) dorsomedial prefrontal cortex (dmPFC) (e.g., Ioannides et al., 2009). Evidence from EEG and intracranial recordings have reported lower frequency (theta-band) activity during REM sleep in the hippocampus and frontal regions, including the ACC and the dorsolateral prefrontal cortex (dlPFC) (Cantero et al., 2003; Simor et al., 2016; Vijayan et al., 2017). Intracranial EEG studies, although more spatially precise than EEG and MEG, are invasive and usually involve clinical populations with specific electrode placements, limiting the generalisability of the findings. Consequently, we currently lack a comprehensive, whole-brain, spatially, and temporally-resolved characterisation of REM sleep in healthy humans.

Of relevance to understanding REM's roles, accruing evidence suggests that it is not a homogeneous state but instead can be divided into 'phasic' and 'tonic' microstates, each exhibiting distinct features. Roughly 20-30% of a REM episode consists of phasic events, characterised by bursts of eye movements, heightened cortical activity, and prominent theta and gamma frequencies on EEG (Aserinsky, 1971; Simor et al., 2020). In contrast, tonic REM is marked by the absence of eye movements, and the presence of alpha and beta waves (Simor et al., 2020). Research suggests that phasic and tonic REM sleep serve distinct functions, with differences in environmental alertness and information processing during these microstates (Simor, 2020; Takahara et al., 2006; Wehrle et al., 2007). Phasic REM sleep may act as an internally focused processing state, potentially facilitating complex cognitive processes (Simor et al., 2016). Therefore, a whole-brain characterisation of REM sleep should examine these microstates individually.

Amongst the frequency bands that appear to define REM sleep, the theta band has been of particular interest in recent research (Boyce et al., 2016, 2017; Hammer et al., 2021; Harrington et al., 2021; Vijayan et al., 2017). Evidence from EEG and intracranial recordings has detected theta-band activity during REM sleep in the hippocampus and frontal regions, including the ACC and the dlPFC (Cantero et al., 2003; Simor et al., 2016; Vijayan et al., 2017). However, theta activity (in the wake state) can originate from multiple regions and neural circuits, including the hippocampus, extra-hippocampal structures such as the septal complex, entorhinal cortex, and pedunculopontine tegmentum, as well as cortical regions like the medial prefrontal

cortex (mPFC) (Pignatelli, Beyeler, & Leinekugel, 2012). A whole-brain characterisation of REM sleep should be sufficiently spatially precise to differentiate these sources, and to probe the signal characteristics within specific regions.

Theta activity has been particularly implicated in memory consolidation, suggesting a potential mechanism through which REM sleep contributes to this process (Boyce et al., 2016; Nishida et al., 2009; Popa et al., 2010). In one of the few causal studies on this topic, Boyce et al. (2016) demonstrated that optogenetic suppression of medial septum neurons, which generate and pace theta rhythms during REM sleep, impaired memory for object recognition and contextual fear in mice. While this study provided a direct causal link between theta oscillations and memory consolidation, how these neural mechanisms directly translate to humans remains unclear (Boyce et al., 2017). Human studies have suggested that REM sleep is particularly important for emotional memory consolidation. For example, in an EEG study, Nishida et al. (2009) found that prefrontal theta activity during REM sleep predicted the extent of emotional (but not neutral) memory consolidation. This finding led researchers to propose that theta rhythms during REM sleep may facilitate the offline interaction and encoding of disparate brain regions, enhancing the consolidation of emotional memories (Nishida et al., 2008; Goldstein & Walker, 2014).

Understanding theta's role in REM sleep processes could benefit from studying frontal theta activity in humans during wakefulness, based on the idea that neural networks interconnecting particular brain structures and subserving related functions are constrained by the biological properties of their neural substrates. Frontal theta activity in demanding cognitive tasks and resting states has been well-documented (Albouy et al., 2017; Cantero et al., 2003; Capilla et al., 2022; Maurer et al., 2015; Niso et al., 2016). For example, working memory — the cognitive process responsible for the temporary holding and manipulation of information — has been linked to frontal midline theta oscillations in humans (for a review, see Hsieh & Ranganath, 2014). It is compelling to speculate that prefrontal cortical theta oscillations in working memory and those observed during REM sleep involve related cognitive functions, for example in generating and holding in mind sensory and declarative memory as might occur in dreaming (Chow et al., 2013). While testing such a hypothesis would likely involve a series

of dedicated experiments using a wide range of neuroscience techniques and tools, a valuable starting point would be to analyse the similarities between frontal theta patterns in (phasic and tonic) REM sleep and those produced during known cognitive processes, such as working memory.

To firmly establish the roles of REM (and specifically theta) in humans, causal methods will be necessary. Recent advances in techniques such as closed-loop auditory stimulation (CLAS) show promise in influencing REM theta activity non-invasively, raising the hope for new avenues to investigate REM sleep electrophysiology and its relationship to behaviour (Harrington et al., 2021). As described above, the scalp-recorded EEG activity likely represents a mixture of activity from multiple neural sources; measuring theta at a single electrode site is likely to be inexact. Another motivation for a whole-brain characterisation of REM theta is therefore to identify neural targets for future causal manipulation.

MEG is ideally suited for investigating the oscillatory patterns of REM sleep in intact humans, as it involves silent, passive recording and combines the high temporal resolution of EEG with decent spatial resolution (Baillet et al., 2017). Only a few early studies have investigated REM sleep using MEG, primarily focusing on brain activity related to REM eye movements (e.g., Ioannides et al., 2004; Corsi-Cabrera et al., 2008). MEG techniques have advanced significantly in the last decade, particularly with the development of distributed source analysis techniques, which have enabled more precise spatial localisation of neural activity (Baillet et al., 2017). While MEG data analyses have mainly focused on cortical activity, recent work has demonstrated that neural activity from deeper, subcortical brain regions can be measured (e.g., Coffey et al., 2016). MEG is well-suited for mapping the temporal dynamics of neural substrates underlying REM sleep, offering insights into their functions and contributions to cognitive processes, including memory consolidation.

1.1 Aims and objectives

This work presents a comprehensive whole-brain topographical mapping of REM oscillatory activity using MEG. The main objectives of this study are as follows:

1. To identify and distinguish theta activity from potential overlapping bands, such as alpha.

2. To characterise the spatiotemporal patterns of theta specific to REM sleep and its microstates
3. To investigate the similarities in theta rhythms between REM sleep and working memory.

Towards these ends, we recorded MEG/EEG data simultaneously in an overnight design in 10 healthy subjects. We also processed an existing dataset of similar MEG/EEG data collected from 17 healthy young adults as they performed an auditory working memory task, for a direct comparison to theta activity generated during REM sleep, using identical methods. We believe that the results will be useful for advancing our understanding of REM sleep's functional significance and its role in memory consolidation.

Methods

Participants

1.1.1 Sleep study

We obtained EEG/MEG recordings during nocturnal sleep from 10 healthy participants who were selected for being comfortable in a supine sleeping position. The subjects' age range was 20-28 (mean: 25.1, SD: 2.6), and six were female. Subjects reported having no sleep-related disorders, not to have changed time zones in the 6 weeks preceding the experiment, and not to be engaged in shift-work. Chronotype was assessed with the Munich Chronotype Questionnaire to adjust the sleep period to the subject's habitual sleep rhythm. Participants were asked to get up an hour earlier than usual on experimental days, to refrain from napping, and to abstain from consuming alcohol, caffeine, or other substances affecting central nervous system function. The study was approved by the Ethics commission of the Universitätsklinikum Tübingen, and written informed consent was obtained for all subjects.

1.1.2 Working memory study

We obtained a separate dataset of MEG/EEG recordings from participants performing an auditory working memory task (Albouy et al., 2017). The study involved 17 healthy participants,

including five females (mean age: 28.12, SD: 3.86 years; range: 21-33 years). All participants reported normal hearing and no history of neurological or psychiatric disorders. They provided written informed consent and received monetary compensation for their participation. Each participant underwent a preliminary session to check for potential MEG artefacts. Ethical approval was obtained from the Ethics Review Board of the Montreal Neurological Institute (NEU-14-043) and the Comité d'Éthique de la Recherche en Arts et en Sciences of Université de Montréal (CERAS-2014-15-251-D), and written informed consent was obtained for all subjects.

General experimental design

1.1.3 Sleep study

Each subject slept in the MEG scanner for a total of five nights as part of a learning study with other experimental objectives; one adaptation night, followed immediately by the first experimental night. Three subsequent experimental nights took place with intervals of about a week. For the present analysis, one complete experimental night was analysed for each subject, selected according to availability at the time of analysis. On experimental nights, subjects came to the MEG centre 3 hours before their sleep time, changed into comfortable sleeping clothes, and were fitted with electrodes. They performed a learning task involving photographs presented at different screen locations (results not reported herein) followed by a memory retrieval task, while seated in the MEG scanner for approximately an hour. The MEG system was then moved to a supine orientation and furnished with bedding, cushioned pads were placed so as to limit head movement, and the lights were turned off. Subjects were awakened after approximately 6 hours of sleep, counted from the first K-complex (slow oscillation) or sleep spindle observed in the EEG recording.

1.1.4 Working memory study

The working memory study involved Transcranial Magnetic Stimulation (TMS); however, our analyses examined data exclusively from the sham condition (i.e., no active TMS session). Participants performed two auditory melodic discrimination tasks: simple melodies and ma-

nipulation melodies. Both of these tasks involved detecting if the pitch of a single tone among a series of 3 tones changed in the second melody (with pitch changes of 2 or 3 semitones). In the simple task, participants compared two melodies to determine if a single tone in the second melody was altered. In the manipulation task, the tones of the second melody were rearranged so that the final tone became the first. We used data from both the simple and manipulation tasks to enhance the robustness and reliability of our analyses by providing a larger number of trials; the difference as regards brain activity lies in stronger activation of the left intra-parietal sulcus, a brain region that is involved specifically in transforming mental representations, in the manipulation condition observed in direct comparison between the conditions (see Albouy et al., 2017 for additional details).

EEG and MEG measurement

For the sleep study, polysomnography (PSG) and MEG data were simultaneously recorded and synchronised using a CTF MEG system (Omega 275, CTF MEG Neuro Innovations Inc.) and its in-built EEG system. PSG was recorded using 12 electrodes at a sampling frequency of 1171.9 Hz, including EEG at C3 and C4 (10–20 International System), electromyogram (left and right jaw muscle), electrooculogram (horizontal and vertical), and electrocardiogram. A reference electrode was affixed to the nose, and the ground electrode was placed on the collarbone. MEG data were recorded from 270 channels (axial gradiometers). Head position was tracked using three head position indicator coils placed anterior to the ears and in the centre of the forehead. Head shape was digitised using a Polhemus Isotrak (Polhemus Inc., VT, USA) for alignment with the subject's anatomical T1-weighted MRI. For the auditory working memory study, the same CTF MEG system was used, but without PSG recording. The sampling rate was set to 1200 Hz with a filter bandwidth of 0–150 Hz. EEG data were acquired from 62 channels. Positions of the EEG electrodes were estimated using the same digitizer system (Polhemus Isotrak).

Anatomical basis of distributed source models

For both the sleep and working memory studies, T1-weighted 1mm³ isotropic MRI images were acquired to maximise the accuracy of source reconstruction. In one subject from the sleep study, the MRI was unavailable, so a standard MNI152 brain was used as a substitute, with the relative location of fiducial points estimated using photographs and head anatomy. MRI scans were automatically segmented using Freesurfer and imported into Brainstorm to serve as the basis for anatomical source modelling (Fischl, 2012).

Sleep scoring

The PSG data were preprocessed (band-pass filtered 0.1-40 Hz), and used to score sleep according to Rechtschaffen and Kales' criteria, in which 30 second epochs are visually inspected and divided into REM, stage 2 sleep (N2), stage 3 (N3) and stage 4 (N4) sleep (noting that most researchers no longer distinguish between N3 and N4 stages; these were combined for subsequent analyses). Two raters independently scored each night's sleep, based on the C4 electrode. A third rater then reviewed the two and reconciled any discrepancies, and then performed a finer-grained scoring of shorter epochs. Specifically, we selected 5 s non-overlapping windows that were free of movement artefacts and which best and unambiguously represented the sleep stages and substages of interest. For REM, epochs were identified which either clearly contained eye movements ('REM phasic') or no eye movements ('REM tonic'). In 30 s epochs classified as N2 sleep, 3 types of epochs were marked: those in which a spindle occurred but not a K-complex ('N2 Spindle'), those in which a K-complex occurred ('N2 K-complex'), and those in which neither was evident ('N2 Plain'). In 30 s epochs classified as either N3 or N4, 5 s windows in which clear slow wave activity (i.e. high amplitude, 0.5-2 Hz oscillations) was evident for the full duration were selected (slow wave sleep; 'SWS'). These selected epochs were not continuous sub-classifications of the 30 s sleep stages-classification, but rather represented a smaller subset of the most representative neural activity for each sub-stage; the total number of epochs included by sleep sub-stages in the analysis is reported in Table 1.

MEG sleep analysis

Data analysis was performed with Brainstorm (Tadel et al., 2011), and using custom MATLAB scripts (The Mathworks Inc., MA, USA). Cardiac artefacts were removed using Brainstorm's in-built source signal space projection algorithm, using the recommended procedure: projectors were removed when they captured at least 10% of the variance of the signal and the topography matched those of cardiac origin upon visual inspection. Artefacts caused by eye movements were not removed for this sleep data analysis, as they do not occur in NREM sleep, and because REMs are highly correlated with REM neural activity (Miyachi et al., 2009), increasing the risk of removing or distorting relevant oscillatory activity. Data were then filtered between 0.1-100 Hz, notch filtered at 50 Hz (power line noise), downsampled to 500 Hz, and epoched based on the PSG analysis described above. Using the imported Freesurfer brain segmentation, an overlapping spheres volume head model was computed for each subject based on a regular isotropic 5 mm grid. This forward model explains how an electric current flowing in the brain would be recorded at the level of the sensors, with fair accuracy (Tadel et al., 2011). A noise covariance matrix was computed from 2 min empty room recordings taken before each session for 6 subjects. Recordings were not available for four datasets; we used instead an average computed from the others (these strongly resembled one another as all data were collected on the same instrument during the same time period). The inverse imaging model estimates the distribution of brain currents that accounts for data recorded at the sensors. We computed the MNE source distribution with unconstrained sources and default Brainstorm parameters for each epoch (Gramfort et al., 2014). The MNE source model is simple, robust to noise and model approximations, are very frequently used in literature, and has previously been shown them to be sensitive to deep brain sources in the brainstem and thalamus, using a similar analysis pipeline (Coffey et al., 2016; 2021).

Defining regions of interest

We constructed a whole-brain volume atlas for each subject, comprising 415 regions. Cortical and subcortical regions were derived from the Atlas of Intrinsic Connectivity of Homotopic Areas (AICHA), a functional brain atlas derived from resting-state fMRI data (Joliot et al.,

2015). The cerebellum was added using the Automated Anatomical Labelling (AAL) atlas, consisting of 26 regions, including the vermis (Rolls et al., 2020). Additionally, subcortical structures of known relevance to REM sleep were selected a priori on the basis of prior neuroimaging studies described in the Introduction, namely the lateral geniculate nuclei (LGN), the pedunculopontine nucleus (PPN), and the medial septum (Boyce et al., 2016; Gott, Liley, & Hobson, 2017; Rye, 1997). The LGN was created as a volume scout in standard space based on the FSL's Harvard–Oxford Cortical and Subcortical Structural probabilistic atlases with coordinates for the left LGN at $L = -22, -32, 0$ and for the right LGN at $R = 24, -30, 0$ (Desikan et al., 2006). The PPN and medial septum were defined on the on the MNI template with reference to gross anatomy, which was subsequently transformed into native space and visually inspected for alignment with individual anatomy. The PPN ($L = -4.5, -29.7, -17, R = 4.6, -29.7, -16$), each of which (left, right) had a mean volume of 0.096 cm^3 (SD: 0.107). The medial septum was segmented manually according to Butler et al., (2014) (centred at $0.7, 4.7, 1.9$), with a mean volume of 0.552 cm^3 (SD: 0.126). For each analysis, data were extracted for each of three directions produced by the volume-based MEG model (x, y, z), and subjected to spectral according to the research question.

Waking working memory analysis

To compare our sleep data with the topographies of known waking function, we analysed data from 17 healthy young adults performing an auditory working memory task (Albouy et al., 2017). This analysis was done according to the same steps outlined above, with several accommodations; instead of 5 s epochs, we used 3.5 s epochs which was the length of time subjects had to hold auditory stimuli in mind before being probed as to their accuracy, and thus the longest interval without the influence of sensory information. This analysis followed the same steps outlined above, with several adjustments: instead of using 5 s epochs, we used 3.5 s epochs, which corresponded to the time participants had to retain auditory stimuli in memory before being probed for accuracy. This interval represented the longest period without the influence of sensory information. For the statistical analysis, we created a median topography of working memory for each subject. Each subject's working memory topography

was then compared with an averaged median topography from each sleep stage (across all participants in the REM sleep dataset) using the Pearson correlation coefficient. We chose to use correlation analysis because we were primarily interested in identifying similarities between the working memory and sleep stage topographies rather than differences. The Pearson correlation coefficient is a straightforward method for assessing the strength and direction of linear relationships between two continuous variables, making it well-suited for our objective of comparing topographical distributions. To assess the significance of these correlations, we conducted a Wilcoxon signed-rank test, comparing the correlation values to zero, with an alpha level of 0.001. We selected the Wilcoxon signed-rank test due to its suitability for paired comparisons, its non-parametric nature, and its robustness with small sample sizes.

Spectral analysis

For spectral analysis, we used an irregular-resampling auto-spectral analysis (IRASA) algorithm (Wen & Liu, 2016). This method distinguishes between fractal and oscillatory components in the power spectrum of neurophysiological signals based on their temporal and spectral characteristics, which arise from different mechanisms. Since we are interested in the oscillatory activity during sleep, IRASA allows for a clearer observation of true oscillatory peaks in the spectra and has been used to eliminate 1/f noise from EEG power spectra obtained during sleep (Helfrich et al., 2018). We further calculated the percent difference of oscillatory values over fractal values using the following formula:

$$\text{Percent Difference} = \frac{\text{Oscillatory} - \text{Fractal}}{\text{Fractal}} \quad (1)$$

This step normalises oscillatory power for each subject, revealing the less pronounced oscillations typically masked by 1/f noise and reducing the effects of inter-subject variability in EEG/MEG signal strength (Feld et al., 2021). Spectra for each epoch were averaged across the three directions (x, y, z).

Statistical analysis

To analyse REM versus NREM sleep and phasic versus tonic REM microstates, we employed linear mixed-effects modeling (LMEs). This method is suitable for our analysis because it accounts for the nested structure of our data, with thousands of epochs measured within each subject. This is particularly advantageous given our study design, which involves a relatively low number of subjects but a high number of repeated measures per subject (Schielzeth et al., 2020). LME analyses were conducted in R using the *lmerTest* and *emmeans* packages (Bates et al., 2015; Lenth, 2018). For each LME model, we visually inspected the histograms and quantile-quantile (Q-Q) plots of the residuals to check for deviations from normality and homoscedasticity. Deviations were addressed by removing outliers, defined as values lying beyond 1.5 times the interquartile range (i.e., below Q1 and above Q3). LME models were created for each region of interest (ROI), incorporating the condition variable, which depending on the analysis, was either the frequency band or sleep stage, as a fixed effect. To account for repeated measures, subject variability was included as a random effect. We conducted an analysis of variance (ANOVA) on each model to assess the significance of the condition variable. The *emmeans* package was used to perform post-hoc comparisons and identify specific regions where significant differences existed between conditions. To control for multiple comparisons, we applied false discovery rate (FDR) correction. Regions showing significant differences ($p < 0.05$) in oscillatory activity across different conditions were identified. Given the imbalance in the number of NREM and REM epochs, we randomly selected an equal number of NREM epochs to match those in the REM.

1.2 Whole-brain topographies

Two types of whole-brain spatial topographical maps were created depending on the research question. First, we created spatial topographies of the median percent change of oscillatory over fractal activity across all subjects. The colour scale for the median maps was determined based on the minimum and maximum values within the frequency bands of interest for the specific sleep stage being analysed. The working memory topography was also based on this scale. The maximum and minimum values used for all median topographies can be

found in Table 1 in supplementary materials. Second, we created whole-brain topographies of significant F-statistic values obtained from LME models onto the brain. Statistical significance was determined through FDR-corrected p-values, with a significance level (alpha) set at 0.05. The colour scale for these topographies was based on the range of significant F-statistic values. Brain regions that did not reach significance are depicted in grey.

2 Results

2.1 Sleep scoring

Based on standard 30 s sleep scoring criteria, subjects spent an average of 152.4 min in N2 (SD: 14.1), 84.5 min in N3 and N4 combined (SD: 17.2), and 58.4 min in REM (SD: 21.0), indicating that participants were able to sleep successfully in the scanner environment. The mean and standard deviation of the number of 5 s epochs selected as most representative of each sleep sub-stage are presented in Table 1.

Table 1: Mean number of 5 s epochs for each sleep stage across all subjects, with standard deviations.

REM sleep	Mean number of epochs (SD)
Phasic	174.50 (60.03)
Tonic	154.03 (49.05)
REM (combined)	164.40 (55.74)
NREM sleep	Mean number of epochs (SD)
N2 Spindle	143.70 (43.31)
N2 K-Complex	127.20 (33.62)
N2 Plain	175.70 (59.57)
SWS	219.30 (113.02)
NREM (combined)	166.48 (77.89)

2.2 Separating frontal theta and occipital alpha network in REM sleep

Visual inspection of the topographic distribution of REM sleep in the 4-8 Hz theta band (Figure 1A) revealed distinct two regions of higher amplitude activity: one in frontal-central regions and another in posterior areas of the brain, spanning across occipital regions and the cerebellum. Subsequent investigation into the topographical distribution within each frequency of the theta band during REM sleep revealed distinct relationships between these activation patterns and frequency: the fronto-central pattern was prominent at lower frequencies (3-4 Hz), and the occipital area was observed at 8 Hz (Figure 1B). A closer examination of the spectra from representative regions (Figure 1C) showed that while frontal regions have a broader peak in the 5-7 Hz theta range, occipital regions have a sharp peak at 8.5 Hz, slightly inside the alpha band, which has a known occipital topography (Niso et al., 2016) and is likely not to be the theta-band activity of interest in memory consolidation and executive functions. To minimise the risk of conflating theta and alpha activity, we narrowed the theta range to 5-7 Hz for our primary research questions. For a direct statistical comparison of brain regions preferentially exhibiting theta versus alpha band activity during REM sleep, please refer to Appendix A in supplementary materials.

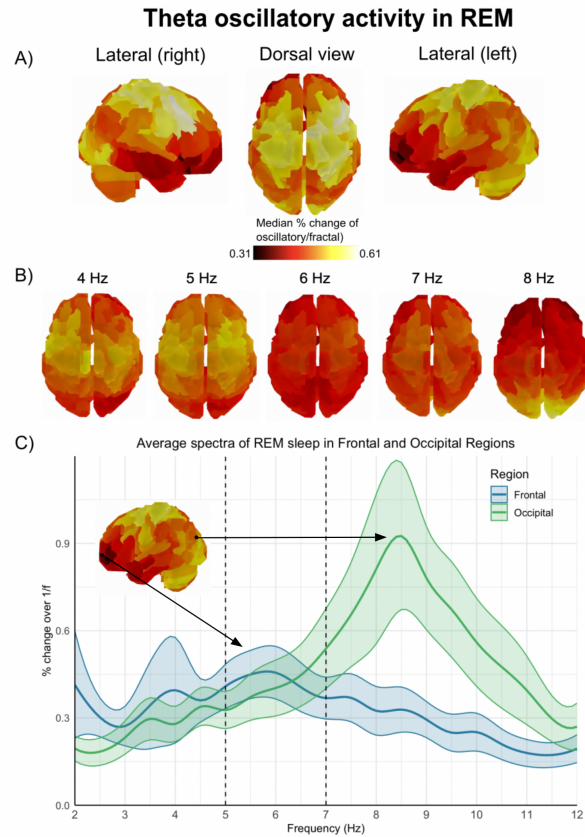


Figure 1: A) Whole-brain topography depicting the median oscillatory activity in the original theta band (4-8 Hz) during REM sleep, combining both phasic and tonic microstates across participants. Visually, two distinct patterns of oscillatory activity emerged: one in frontal-central regions and the other in posterior regions, extending across the occipital lobe and the cerebellum. B) Whole-brain topographical maps of the median oscillatory activity across participants within each frequency of the theta band (dorsal view) revealed a pronounced oscillatory activity pattern in the occipital regions, peaking at 8 Hz, in line with expectations for alpha activity (Niso et al., 2016). C) Average spectra plot of activity in REM sleep in frontal and occipital regions (4-8Hz). The blue and green lines depict the average spectra of a frontal and occipital region, respectively. To reduce the risk of conflating theta and alpha activity, we focused on a narrowed theta range of 5-7 Hz in subsequent analyses (frequency range represented by the dashed lines).

2.3 Comparative analysis of theta patterns in REM sleep

2.3.1 Theta oscillations in REM vs. NREM Sleep

To identify differences in theta activity during REM sleep versus NREM sleep, we conducted an LME analysis at the trial-epoch level, using condition (i.e., REM and NREM) as a fixed effect and subjects as a random effect. The formula used for the analysis was: $\text{value} \sim \text{condition} (1 + \text{condition} | \text{subject})$. The total number

of retained epochs across subjects, after removing outliers and including only values within 1.5 times the IQR from the first and third quartiles, was 2,027,410 (1,023,705 values for each condition). We identified 261 statistically significant regions ($p < 0.05$, FDR corrected) with a greater percent change of oscillatory over fractal activity in the theta band during REM sleep compared to NREM sleep (Figure 2A). Topographical mapping revealed prominent theta activity in frontal-central, superior parietal, and temporal regions during REM sleep (for a list of specific regions, see Table 3 in supplementary materials). Subcortical regions where theta-band activity was significantly greater than alpha-band activity included the hippocampus, medial septum, amygdala, basal ganglia, thalamus, PPN, and LGN (Figure 2B). No activity was observed in occipital or cerebellar regions, indicating that the restricted theta-band range (5-7 Hz) was sufficient to remove occipital alpha activity in REM sleep. No significant differences were found where NREM sleep exhibited greater theta activity than REM sleep.

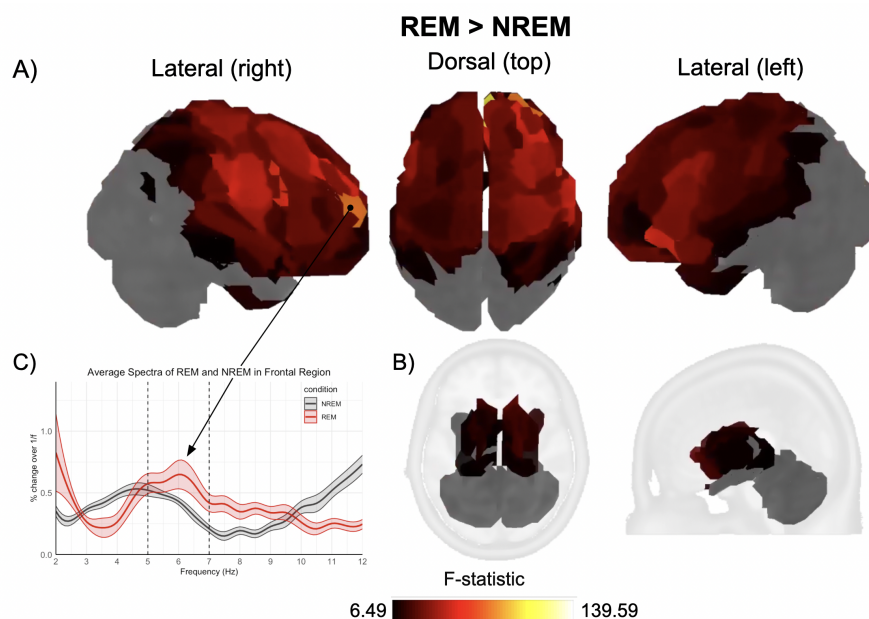


Figure 2: A, B) Whole-brain spatial topography of statistically significant regions of interest showing greater theta activity during REM sleep compared to NREM sleep, as determined by LME models ($p < 0.05$, FDR corrected). No activity in the theta band was observed in the occipital or cerebellar regions, demonstrating that the narrow theta-band range was sufficient to remove occipital alpha activity in REM sleep. Once occipital alpha activity was excluded, theta band activity was stronger over frontal and central regions, as well as subcortical regions including the hippocampus, medial septum, amygdala, basal ganglia (caudate and putamen), thalamus, PPN, and LGN during REM sleep. These findings suggest that activity from these regions in theta could be related to REM's more cognitive roles. C) Average spectra plot of activity in REM and NREM sleep stages in a frontal region (5-7 Hz). The red and black lines depict the average spectra of in REM and NREM sleep stages, respectively.

2.3.2 Theta oscillations in phasic vs. tonic REM sleep

To identify differences in theta activity during phasic and tonic REM microstates, we conducted an LME analysis at the trial-epoch level, using conditions (i.e., phasic and tonic) as fixed effects and subjects as a random effect. The formula used for the analysis was: $\text{value} \sim \text{condition} (1 + \text{condition} | \text{subject})$. The total number of retained epochs across subjects, after removing outliers and including only values within 1.5 times the IQR from the first and third quartiles, was 1,318,128 (659,064 each for each condition). We identified 197 statistically significant regions ($p < 0.05$, FDR corrected) where the percent change of oscillatory over fractal activity in the theta band was greater during tonic REM sleep compared to phasic REM sleep (Figure 3). Theta activity was stronger in the inferior and lateral posterior regions of the brain, in medial anterior frontal regions (for a detailed list of specific regions, see Table 4 in the supplementary materials). In regard to subcortical regions, theta activity was greater in tonic than phasic REM in the medial septum, left hippocampus, left amygdala, basal ganglia, thalamus, PPN, LGN, and the cerebellum. Regions with no significant differences in theta activity between tonic and phasic REM were predominantly located in the superior and medial areas of the brain (note that these regions do show stronger theta activity in the REM vs. NREM comparison, Figure 2). No significant differences were found where phasic REM sleep exhibited greater theta activity than tonic REM sleep.

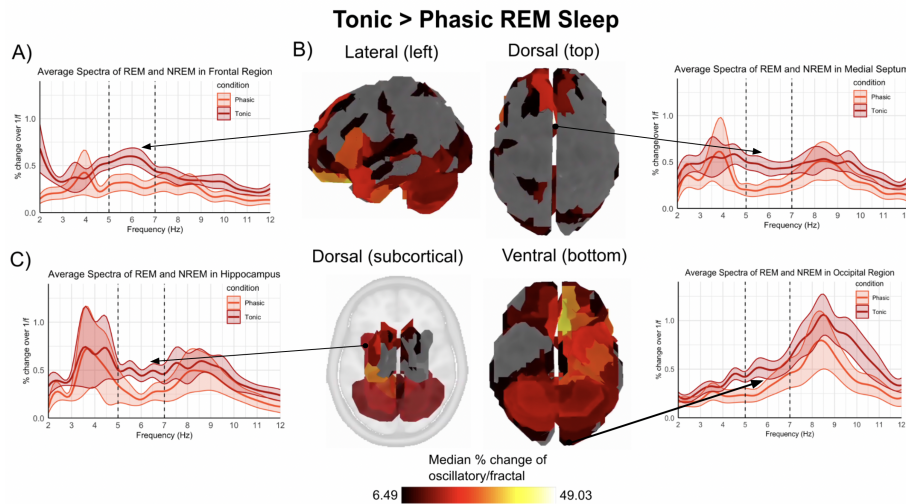


Figure 3: A, C) Average spectra plot of activity in phasic and tonic REM microstates in representative frontal, subcortical (i.e., hippocampus and medial septum), and occipital regions (5-7 Hz). The orange and red lines depict the average spectra of in phasic and tonic states, respectively. The overall amplitude of theta activity (5-7 Hz) is consistently higher in tonic states compared to phasic states in most brain regions. B) Whole-brain spatial topography revealed statistically significant regions with greater theta activity during tonic REM sleep compared to phasic REM sleep, determined by LME models ($p < 0.05$, FDR corrected). No significant differences were found where phasic REM sleep exhibited greater activity than tonic REM sleep. Regions showing greater theta activity in tonic REM sleep were located in the inferior and lateral posterior areas of the brain, as well as in a few anterior regions.

2.4 REM theta versus working memory theta

To compare theta activity during active wakefulness with sleep microstates, we first created group (median) topographies for each condition. Visual inspection of the topographical map of working memory revealed a distinct pattern of theta activity (5-7 Hz) prominent in the frontal and midline regions of the brain (Figure 4, left). A similar pattern was observed during phasic REM sleep, but not in other sleep stages, including tonic REM sleep and NREM sleep stages (i.e., S2 K-complex, S2 Spindle, S2 Plain, and SWS). Next, we used the median topographies from the sleep dataset as templates, correlating them with median brain maps for each subject in the working memory dataset; Pearson correlations were used to quantify the strength of similarity between pairs of maps. Finally, we used the Wilcoxon signed-rank test to evaluate whether similarity differed significantly from that expected by chance levels (alpha level of 0.01). The results indicated that whole-brain theta topographies during the working memory task correlated positively only with phasic REM sleep ($V = 155.00$, $p < 0.001$). Instead, they

correlated negatively with tonic REM sleep ($V = 4.00$, $p < 0.001$) and each NREM sleep stage ($p < 0.001$).

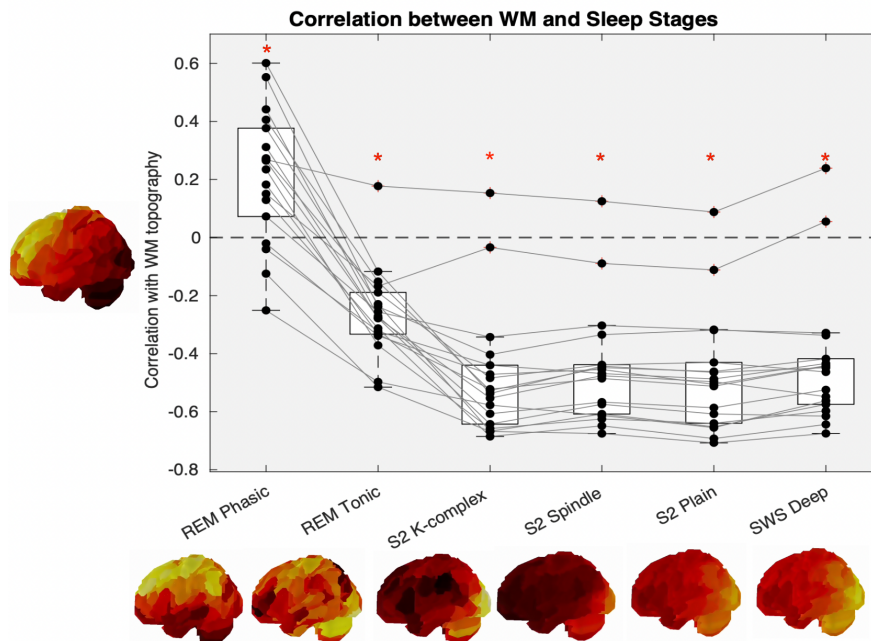


Figure 4: Similarity between each subject’s working memory topography ($N = 17$) and the median topography of each sleep stage across all subjects ($N = 10$). Asterisks indicate similarity (as measured using correlations) which are significantly different from 0 at the group level (alpha level of 0.01, Wilcoxon signed-rank test). There was a positive correlation between working memory and REM phasic sleep, while a negative correlation was found between working memory and all other sleep stages. Both working memory and REM phasic sleep exhibited a prominent frontal and midline pattern, which was not observed in the other sleep stages.

3 Discussion

In this study, we aimed to provide a spatially-resolved, whole-brain characterisation of REM theta activity in healthy human subjects using MEG. Our findings indicated that theta-band activity in the frontal midline regions is best observed by narrowing the theta frequency band to a core range of 5-7 Hz, which allows for better distinction from overlapping alpha-band activity in the occipital and cerebellar regions (Figure 1). Theta-band activity during REM sleep was prominent in frontal, central, temporal, parietal, and subcortical regions (Figure 2). A closer look into REM sleep microstates revealed that theta activity is greater in tonic than phasic REM sleep in inferior and lateral posterior areas (Figure 3). Lastly, similarities were

observed in whole-brain theta topographies between working memory tasks and phasic REM sleep in frontal midline regions; theta topographies during the working memory task correlated positively with phasic REM sleep, and negatively with all other sleep stages (Figure 4).

3.1 Disentangling frontal theta and occipital alpha networks during REM sleep

We first aimed to distinguish the spatiotemporal patterns of theta-band activity from potential overlapping networks, notably in the adjacent alpha range. The majority of previous EEG studies have focused on comparing amplitudes within set frequency ranges rather than examining spatial topographies, thereby overlooking the potential overlap between theta and alpha networks. Theta and alpha networks during REM sleep likely serve distinct functions, as they do during wakefulness (Basar, 2012; Riddle et al., 2020). Our results suggested that the frequency range used in many previous REM sleep studies (4-8 Hz) may capture activity from several neural sources, including occipital areas where activity peaks slightly above the theta range (at 8.5 Hz; see Figure 1C). The distributions of theta and alpha observed in REM sleep strongly resembled those identified in resting wakefulness MEG studies, with theta activity in the frontal regions and alpha in the occipital regions, respectively (Capilla et al., 2022; Niso et al., 2016). The whole-brain topography at 8 Hz (Figure 1B) revealed occipital activity, indicating that what is often considered theta may actually include activity from the alpha band. This overlap could obscure the true spatial patterns and functional roles of theta rhythms during REM sleep, and could make it difficult to target networks with different functions in investigations. A more focused ‘core’ range of 5-7 Hz best captured frontal and midline activity during REM sleep, in agreement with previous EEG studies that have observed frontal theta activity (Simor et al., 2016; Nishida et al., 2009; Vijayan et al., 2017), although some occipital activity was observed in the tonic REM microstate (Figure 3 and 4).

The similarity to wakefulness patterns might imply that similar neural networks are engaged across brain states. The cerebellum exhibited significantly higher alpha activity compared to theta (see Appendix A in supplementary materials). Although the topic of alpha activity is beyond the scope of this paper, a previous PET study has observed activation in this region

(Braun et al., 1997). Simor et al. (2020) found higher alpha activity in tonic REM sleep and suggest that this might be related to external processing. Since tonic REM sleep has been found to partially maintain external processing, this alpha activity could be linked to the same network that maintains alertness during wakefulness. In conjunction with previous work suggesting that theta frequency ranges might differ between human and non-human animals (with the human equivalent of theta-band rodent activity being closer to 1-4 Hz; summarised in Busáki, 2012), and that theta frequency might fluctuate over time according to other physiological processes (Bueno-Junior et al., 2023), our results underscore the need for caution in interpreting amplitude in fixed frequency bands rigidly. New methods may need to be developed to better disentangle spatiotemporal functional brain networks in wake and sleep states (e.g., Yu et al., 2022).

3.2 Characterising theta oscillations in REM sleep

Our primary objective was to identify the distinct spatiotemporal patterns of the theta-band during REM sleep, by directly comparing its oscillatory activity to that of other sleep stages, such as NREM. Previous EEG studies have identified oscillatory activity during REM sleep, but these findings are based on data from a limited number of channels, or from EEG, which offers less spatial accuracy (Simor et al., 2016; Nishida et al., 2009; Baillet et al., 2017). The use of distributed source reconstruction methods in MEG in our study allowed for greater specificity in identifying the spatial distribution of theta activity across the entire brain, including subcortical regions, which are frequently omitted from MEG analyses.

Whole-brain topographies of theta activity during REM sleep revealed a clear pattern of oscillations in the frontal lobe. Our results align with previous EEG and intracranial studies that have observed theta activity in frontal regions such as the dlPFC and ACC during REM sleep (Simor et al., 2016; Nishida et al., 2009; Vijayan et al., 2017). Our results extend these findings by identifying theta rhythms across a wider range of frontal regions, including inferior, medial, middle, and superior frontal regions. This widespread distribution of theta activity may suggest a more integrated role for the frontal lobe in the cognitive processes associated with REM sleep, such as memory consolidation.

Previous PET studies have reported hypoactivation of the dlPFC during REM sleep compared to NREM sleep (Braun et al., 1997; Maquet et al., 2005). However, a recent intracranial EEG study revealed theta-band activity in the dlPFC during REM sleep (Vijayan et al., 2017). The results of our study corroborate these findings, revealing that theta activity in the dlPFC is greater during REM sleep, as compared to NREM sleep. Our findings, along with those of Vijayan et al., 2017, suggest that the dlPFC plays a more significant role in REM sleep than previously understood. During wakefulness, the dlPFC is involved in the maintenance and manipulation of information during working memory tasks (Blumenfeld & Ranganath, 2006; Barbey et al., 2013). For example, increased dlPFC activation during working memory tasks that require rearranging the order of items and in tasks that require chunking, in fMRI studies (Blumenfeld & Ranganath, 2006; Bor et al., 2004). During REM sleep, the function of the dlPFC might be to help the reorganisation of neural representations of experiences to potentially integrate new information with existing memories. Although it is intriguing to consider that the dlPFC may be involved in certain cognitive processes related to memory or dreaming, further research is required before making any conclusions about the precise role that this region may have in relation to REM sleep.

Our study corroborates previous PET studies identifying the neural substrates active during REM sleep, while extending these findings by using MEG to reveal that these regions are specifically oscillating within the theta band. Specifically, our results replicate previous PET studies comparing REM to NREM sleep by identifying theta activity in regions such as the anterior cingulate cortex, frontal medial cortex, fusiform gyrus, insula, parahippocampal gyrus, precuneus, supplementary motor area, temporal gyrus, and temporal pole (Braun et al., 1997; Maquet et al., 2005). While the precise functional role of these theta oscillations remains to be understood, from a cognitive perspective, this widespread activity may support the integration of certain cognitive processes, potentially facilitating memory consolidation and the integration of new learning with prior knowledge, and/or other higher-order brain functions during REM sleep.

Investigating deep subcortical sources using MEG is a relatively new method. Initially, it was believed that MEG could only effectively localise cortical sources because deeper sources

produce signals that are more attenuated by their central location relative to the sensor helmet and distance from source to sensors (Hämäläinen et al., 1993). However, recent studies have developed methods to resolve these deep sources, detecting activity in the cerebellum, thalamus, and brainstem (Andersen et al., 2020; Coffey et al., 2016; 2021). Our results demonstrate that it is possible to record theta activity during REM sleep in subcortical structures, including the amygdala, basal ganglia, hippocampus, medial septum, PPN, LGN, and thalamus. Most of the regions where we observed theta activity are known to be crucial for REM sleep. For example, the hippocampus and medial septum are essential for memory processing and the synchronisation of theta rhythms (Boyce et al., 2016). The hippocampus and amygdala play important roles in the expression of drive and affect, as well as in the control of autonomic function (Braun et al., 1997). The PPN and thalamus are involved in REM initiation and maintenance, contributing to the generation and modulation of REM sleep-associated neural activity (Urbano et al., 2014). The LGN is associated with processing visual information during REM sleep (particularly in relation to ponto-geniculo-occipital (PGO) waves), while the basal ganglia are involved in motor control and the regulation of sleep-wake transitions (Steriade et al., 1989; Braun et al., 1997). The results presented here highlight MEG's potential as a tool for exploring spatiotemporal patterns across the entire brain in healthy humans and further investigating the functional contributions of subcortical brain regions across brain states.

Examining REM sleep microstates more closely, we found that theta oscillations in tonic REM appear more prominently in inferior and lateral posterior areas than they do in phasic REM. This result is best interpreted in conjunction with the REM vs. NREM result (Figure 2) and with reference to the group topographies displayed in Figure 4: REM in general as compared with NREM is characterised by theta-band activity over frontal and dorsal cortical structures, yet these are less regionally-concentrated in tonic vs. phasic microstates, with theta in tonic REM observed in wider selection of ventral regions. Extracting spectra from representative regions during each microstate offers further insight: in both a frontal cortical region (Figure 3) and an occipital region, tonic REM has slightly higher oscillatory activity in the 5-7 Hz range than does phasic REM. In some subcortical regions (medial septum, hippocampus), theta activity appears to have two peaks; one at 2-4 Hz and the other at 8-9 Hz;

this pattern is more distinct in phasic REM (in accordance with previous work, Simor et al., 2020), whereas tonic REM exhibited somewhat elevated activity across the intervening range, which includes our 5-7 Hz focus. These results support the idea that tonic and phasic periods in REM state are distinct states (Simor et al., 2020), further nuance our understanding of theta sources given that the analysis used here has separated oscillatory activity from fractal activity (which can change across brain state; Wen & Liu, 2016; Lendner et al., 2020), demonstrate that MEG can be used to observe fine-grained patterns in frequency of subcortical brain regions, and provide suggestions for where to look for further differences between microstates. For example, our results suggest that a special feature of phasic REM might actually be 2-4 Hz activity rather than theta, and that it might be generated in subcortical regions including hippocampus and medial septum. As these regions are causally implicated in memory consolidation in animal models (Boyce et al., 2019), and human theta might be lower in frequency than in rodents (Busáki, 2012), it is possible that this lower frequency band (potentially coupled to gamma-band activity) is involved in coordinating transfer of spatial and temporally-organised information with the hippocampus (Nuñez and Bruno, 2021), whereas cortical theta over a broader frequency range is engaged in other processes such as integrating the information with previous knowledge.

3.3 The similarities between REM theta and working memory theta

We observed a high similarity in theta topography between phasic REM sleep and waking working memory; both showed a pattern of stronger activity in frontal midline areas (Figure 4). This similarity was observed only for phasic REM sleep. The working memory pattern correlated negatively with all other sleep microstates, including tonic REM sleep. The exclusive similarity observed between theta activity during phasic REM sleep and working memory tasks in wakefulness suggests that a frontal theta network may serve similar functions in both states, and that network activity might be suppressed in NREM sleep, in which only the occipital alpha-like pattern was observed.

Theta activity associated with working memory processes has previously been observed in frontal midline regions (Hsieh and Ranganath, 2014). In sleep, external stimuli and en-

environmental alertness is relatively preserved in tonic REM sleep, and is decreased in phasic REM sleep (Simor et al., 2020). This distinction suggests that phasic REM sleep serves as an internally-focused processing state, potentially facilitating complex cognitive processes. Additionally, previous studies have shown that theta activity is more prominent in phasic than in tonic REM sleep (Simor et al., 2016). Given that phasic REM sleep appears to support internal cognitive processes and that theta activity is prominent during this microstate, it could be an important period for activities related to cognitive processes including memory consolidation.

Furthermore, the activation of working memory-like networks during phasic REM sleep could support the reorganisation and integration of memories. Although we did not observe strong patterns of functional connectivity between dlPFC and other REM-related brain regions of interest, as mentioned, the dlPFC plays a crucial role in maintaining and manipulating information during working memory tasks (Blumenfeld & Ranganath, 2006; Barbey et al., 2013). The presence of theta oscillations in the dlPFC during phasic REM sleep suggests that similar mechanisms might be at play. For example, theta activity in frontal regions may be critical for reorganising neural representations of experiences and integrating new information with existing memories. The involvement of the dlPFC in these processes during REM sleep could aid in refining and stabilising memory traces. In memory models of sleep, the Sequential Hypothesis of Memory Consolidation suggests that NREM sleep strengthens individual memory traces, while REM sleep integrates these traces into existing knowledge networks (Guiditta, 2014). During REM sleep, the activation of neural networks similar to those involved in working memory may promote the reorganisation of neural representations. This reorganisation may support the integration of new information with pre-existing memories, thereby enhancing the overall consolidation process.

3.4 Limitations

Our sample size for the sleep analysis is relatively small ($N = 10$). To address this limitation, we employed linear mixed-effects models (LMEs) to account for the nested structure of our data, which includes thousands of epochs per subject. This statistical approach is particularly advantageous for our study design, as it allowed us to capitalise on the extensive data from

each subject, thereby enhancing the robustness and validity of the results (Schielzeth et al., 2020). Furthermore, our study focuses specifically on the electrophysiological features of sleep, which generally exhibits less variability compared to behavioural studies. While the study's physiological focus is a strength as regards obtaining high SNR within a small sample, the study design is of a passive, observational nature; we have not manipulated REM theta, and so our interpretation as regard theta function similar remain correlational and speculative. We nonetheless believe that characterising REM theta in healthy humans is an important and necessary precursor to these more mechanistic investigations.

4 Conclusion

Using MEG, we were able to capture the frequency-specific activity of brain regions during REM sleep, identifying the spatiotemporal patterns of theta oscillations, including in deep subcortical sources. These findings can help guide future studies in several ways. Future research can use closed-loop adaptive stimulation (CLAS) and other brain stimulation techniques to offer causal insights into the role of theta oscillations in REM sleep. For instance, subsequent experimental studies could target prefrontal theta activity using CLAS to modulate and enhance memory consolidation processes. By applying stimulation during REM sleep when theta activity is naturally occurring, researchers could investigate how altering theta rhythms impacts memory consolidation (Harrington et al., 2021). Subsequent investigations using MEG should investigate other frequency bands of interest in REM sleep, including delta, beta and gamma oscillations, as well as theta-gamma coupling. Theta-gamma coupling has been observed during both REM sleep and working memory tasks in the hippocampus and neocortex (Bandarabadi et al., 2019; Scheffzük et al., 2011; Tamura et al., 2017). A better understanding of this coupling could reveal how frontal regions in REM sleep function similarly to those during working memory, or perhaps that subcortical but not cortical theta is coupled to gamma oscillations. Lastly, there is limited research on the cerebellum's role in REM sleep (see Canto et al., 2017 for a review). We observed theta activity within the cerebellum during REM sleep, aligning with a previous study that reported cerebellar activation (Braun et al., 1997).

The cerebellum's role in sleep has recently started to gain interest after the discovery that it generates sleep spindles, which are hallmarks of memory consolidation in NREM sleep (Xu et al., 2021). Our results showing different patterns of activity in the cerebellum across sleep states (Figure 4) further support that MEG can be used to study cerebellar activity (Andersen et al., 2020), and open new possibilities to explore its role in sleep and memory (Benarroch, 2023; Jackson & Xu, 2023).

There is much to be done to precisely define the role of REM sleep and its underlying neural mechanisms in sleep-dependent memory consolidation. This work contributes a whole-brain characterisation of the spatiotemporal patterns of theta rhythms in healthy humans to these efforts, and suggests targets and tools for further exploration.

References

- Albouy, P., Weiss, A., Baillet, S., & Zatorre, R. J. (2017). Selective entrainment of theta oscillations in the dorsal stream causally enhances auditory working memory performance. *Neuron*, *94*(1), 193-206. <https://doi.org/10.1016/j.neuron.2017.03.015>
- Achermann, P., Rusterholz, T., Dürr, R., König, T., & Tarokh, L. (2016). Global field synchronization reveals rapid eye movement sleep as most synchronized brain state in the human EEG. *Royal Society open science*, *3*(10), 160201. <https://doi.org/10.1098/rsos.160201>
- Adamantidis, A. R., Gutierrez Herrera, C., & Gent, T. C. (2019). Oscillating circuitries in the sleeping brain. *Nature Reviews Neuroscience*, *20*(12), 746-762. <https://doi.org/10.1038/s41583-019-0223-4>
- Andersen, L. M., Jerbi, K., & Dalal, S. S. (2020). Can EEG and MEG detect signals from the human cerebellum? *NeuroImage*, *215*, 116817. <https://doi.org/10.1016/j.neuroimage.2020.116817>
- Baillet, S. (2017). Magnetoencephalography for brain electrophysiology and imaging. *Nature Neuroscience*, *20*(3), 327-339.
- Bandarabadi, M., Boyce, R., Gutierrez Herrera, C., Bassetti, C. L., Williams, S., Schindler, K., & Adamantidis, A. (2019). Dynamic modulation of theta–gamma coupling during rapid eye movement sleep. *Sleep*, *42*(12), zsz182. <https://doi.org/10.1093/sleep/zsz182>
- Barbey, A. K., Koenigs, M., & Grafman, J. (2013). Dorsolateral prefrontal contributions to

- human working memory. *Cortex*, 49(5), 1195-1205.
<https://doi.org/10.1016/j.cortex.2012.05.022>
- Başar, E. (2012). A review of alpha activity in integrative brain function: fundamental physiology, sensory coding, cognition and pathology. *International Journal of Psychophysiology*, 86(1), 1-24.
- Bates, D., Maechler, M., Bolker, B., Walker, S., Christensen, R. H. B., Singmann, H., ... & Bolker, M. B. (2015). Package 'lme4'. *Convergence*, 12(1), 2.
- Benarroch, E. (2023). What is the involvement of the cerebellum during sleep?. *Neurology*, 100(12), 572-577.
<https://doi.org/10.1212/WNL.0000000000207161>
- Blumenfeld, R. S., & Ranganath, C. (2006). Dorsolateral prefrontal cortex promotes long-term memory formation through its role in working memory organization. *Journal of Neuroscience*, 26(3), 916-925. <https://doi.org/10.1523/JNEUROSCI.2353-05.2006>
- Bor, D., Cumming, N., Scott, C. E., & Owen, A. M. (2004). Prefrontal cortical involvement in verbal encoding strategies. *European Journal of Neuroscience*, 19(12), 3365-3370.
<https://doi.org/10.1111/j.1460-9568.2004.03438.x>
- Boyce, R., Glasgow, S. D., Williams, S., & Adamantidis, A. (2016). Causal evidence for the role of REM sleep theta rhythm in contextual memory consolidation. *Science*, 352(6287), 812-816. <https://doi.org/10.1126/science.aad5252>
- Boyce, R., Williams, S., & Adamantidis, A. (2017). REM sleep and memory. *Current Opinion in Neurobiology*, 44, 167-177. <https://doi.org/10.1016/j.conb.2017.05.001>

- Braun, A. R., Balkin, T. J., Wesenten, N. J., Carson, R. E., Varga, M., Baldwin, P., ... & Herscovitch, P. (1997). Regional cerebral blood flow throughout the sleep-wake cycle. An H₂ (15) O PET study. *Brain: a journal of neurology*, *120*(7), 1173-1197.
<https://doi.org/10.1093/brain/120.7.1173>
- Braun, A. R., Balkin, T. J., Wesensten, N. J., Gwadrý, F., Carson, R. E., Varga, M., ... & Herscovitch, P. (1998). Dissociated pattern of activity in visual cortices and their projections during human rapid eye movement sleep. *Science*, *279*(5347), 91-95.
<https://doi.org/10.1126/science.279.5347.91>
- Brodts, S., Inostroza, M., Niethard, N., & Born, J. (2023). Sleep—A brain-state serving systems memory consolidation. *Neuron*, *111*(7), 1050-1075.
<https://doi.org/10.1016/j.neuron.2023.03.005>
- Bueno-Junior, L. S., Ruckstuhl, M. S., Lim, M. M., & Watson, B. O. (2023). The temporal structure of REM sleep shows minute-scale fluctuations across brain and body in mice and humans. *Proceedings of the National Academy of Sciences*, *120*(18), e2213438120.
<https://doi.org/10.1073/pnas.2213438120>
- Butler, T., Zaborszky, L., Pirraglia, E., Li, J., Wang, X. H., Li, Y., ... & Thesen, T. (2014). Comparison of human septal nuclei MRI measurements using automated segmentation and a new manual protocol based on histology. *Neuroimage*, *97*, 245-251. <https://doi.org/10.1016/j.neuroimage.2014.04.026>
- Buzsáki, G., & Watson, B. O. (2012). Brain rhythms and neural syntax: implications for efficient coding of cognitive content and neuropsychiatric disease. *Dialogues in clinical neuroscience*, *14*(4), 345-367. <https://doi.org/10.31887/DCNS.2012.14.4/gbuzsaki>

- Cantero, J. L., Atienza, M., Madsen, J. R., & Stickgold, R. (2004). Gamma EEG dynamics in neocortex and hippocampus during human wakefulness and sleep. *NeuroImage*, 22(3), 1271-1280. <https://doi.org/10.1016/j.neuroimage.2004.03.014>
- Cantero, J. L., Atienza, M., Stickgold, R., Kahana, M. J., Madsen, J. R., & Kocsis, B. (2003). Sleep-dependent θ oscillations in the human hippocampus and neocortex. *Journal of Neuroscience*, 23(34), 10897-10903. <https://doi.org/10.1523/JNEUROSCI.23-34-10897.2003>
- Capilla, A., Arana, L., García-Huésca, M., Melcón, M., Gross, J., & Campo, P. (2022). The natural frequencies of the resting human brain: An MEG-based atlas. *NeuroImage*, 258, 119373. <https://doi.org/10.1016/j.neuroimage.2022.119373>
- Cape, E. G., Manns, I. D., Alonso, A., Beaudet, A., & Jones, B. E. (2000). Neurotensin-induced bursting of cholinergic basal forebrain neurons promotes γ and θ cortical activity together with waking and paradoxical sleep. *Journal of Neuroscience*, 20(22), 8452-8461. <https://doi.org/10.1523/JNEUROSCI.20-22-08452.2000>
- Canto, C. B., Onuki, Y., Bruinsma, B., van der Werf, Y. D., & De Zeeuw, C. I. (2017). The sleeping cerebellum. *Trends in Neurosciences*, 40(5), 309-323. <https://doi.org/10.1016/j.tins.2017.03.001>
- Chong-Hwa Hong, C., Gillin, J. C., Dow, B. M., Wu, J., & Buchsbaum, M. S. (1995). Localized and lateralized cerebral glucose metabolism associated with eye movements during REM sleep and wakefulness: a positron emission tomography (PET) study. *Sleep*, 18(7), 570-580. <https://doi.org/10.1093/sleep/18.7.570>

- Chow, H. M., Horowitz, S. G., Carr, W. S., Picchioni, D., Coddington, N., Fukunaga, M., ... & Braun, A. R. (2013). Rhythmic alternating patterns of brain activity distinguish rapid eye movement sleep from other states of consciousness. *Proceedings of the National Academy of Sciences*, *110*(25), 10300-10305.
<https://doi.org/10.1073/pnas.1217691110>
- Coffey, E. B., Arseneau-Bruneau, I., Zhang, X., Baillet, S., & Zatorre, R. J. (2021). Oscillatory entrainment of the frequency-following response in auditory cortical and subcortical structures. *Journal of Neuroscience*, *41*(18), 4073-4087.
<https://doi.org/10.1523/JNEUROSCI.2313-20.2021>
- Coffey, E. B., Herholz, S. C., Chepesiuk, A. M., Baillet, S., & Zatorre, R. J. (2016). Cortical / contributions to the auditory frequency-following response revealed by MEG. *Nature Communications*, *7*(1), 11070. <https://doi.org/10.1038/ncomms11070>
- Corsi-Cabrera, M., Guevara, M. A., & del Río-Portilla, Y. (2008). Brain activity and temporal coupling related to eye movements during REM sleep: EEG and MEG results. *Brain research*, *1235*, 82-91. <https://doi.org/10.1016/j.brainres.2008.06.052>
- De Carli, F., Proserpio, P., Morrone, E., Sartori, I., Ferrara, M., Gibbs, S. A., ... & Nobili, L. (2016). Activation of the motor cortex during phasic rapid eye movement sleep. *Annals of Neurology*, *79*(2), 326-330. <https://doi.org/10.1002/ana.24556>
- Desikan, R. S., Ségonne, F., Fischl, B., Quinn, B. T., Dickerson, B. C., Blacker, D., ... & Killiany, R. J. (2006). An automated labeling system for subdividing the human cerebral cortex on MRI scans into gyral based regions of interest. *Neuroimage*, *31*(3), 968-980.

- Diekelmann, S., & Born, J. (2010). The memory function of sleep. *Nature Reviews Neuroscience*, *11*(2), 114-126. <https://doi.org/10.1038/nrn2762>
- Feld, G. B., Bergmann, T. O., Alizadeh-Asfestani, M., Stuke, V., Wriede, J. P., Soekadar, S., & Born, J. (2021). Specific changes in sleep oscillations after blocking human metabotropic glutamate receptor 5 in the absence of altered memory function. *Journal of Psychopharmacology*, *35*(6), 652-667. <https://doi.org/10.1177/02698811211005627>
- Fernandez, L. M., & Lüthi, A. (2020). Sleep spindles: mechanisms and functions. *Physiological Reviews*, *100*(2), 805-868. <https://doi.org/10.1152/physrev.00042.2018>
- Fischl, B. (2012). FreeSurfer. *NeuroImage*, *62*(2), 774-781. <https://doi.org/10.1016/j.neuroimage.2012.01.021>
- Gramfort, A., Luessi, M., Larson, E., Engemann, D. A., Strohmeier, D., Brodbeck, C., ... & Hämäläinen, M. S. (2014). MNE software for processing MEG and EEG data. *NeuroImage*, *86*, 446-460. <https://doi.org/10.1016/j.neuroimage.2013.10.027>
- Goldstein, A. N., & Walker, M. P. (2014). The role of sleep in emotional brain function. *Annual review of clinical psychology*, *10*(1), 679-708.ta
- Gott, J. A., Liley, D. T., & Hobson, J. A. (2017). Towards a functional understanding of PGO waves. *Frontiers in Human Neuroscience*, *11*, 89. <https://doi.org/10.3389/fnhum.2017.00089>
- Giuditta, A. (2014). Sleep memory processing: the sequential hypothesis. *Frontiers in systems neuroscience*, *8*, 219. <https://doi.org/10.3389/fnsys.2014.00219>
- Hsieh, L. T., & Ranganath, C. (2014). Frontal midline theta oscillations during working

- memory maintenance and episodic encoding and retrieval. *Neuroimage*, 85, 721-729.
<https://doi.org/10.1016/j.neuroimage.2013.08.003>
- Hammer, M., Schwale, C., Brankač, J., Draguhn, A., & Tort, A. B. (2021). Theta-gamma coupling during REM sleep depends on breathing rate. *Sleep*, 44(12), zsab189.
<https://doi.org/10.1093/sleep/zsab189>
- Harrington, M. O., Ashton, J. E., Ngo, H. V. V., & Cairney, S. A. (2021). Phase-locked auditory stimulation of theta oscillations during rapid eye movement sleep. *Sleep*, 44(4), zsaa227. <https://doi.org/10.1093/sleep/zsaa227>
- Helfrich, R. F., Mander, B. A., Jagust, W. J., Knight, R. T., & Walker, M. P. (2018). Old brains come uncoupled in sleep: slow wave-spindle synchrony, brain atrophy, and forgetting. *Neuron*, 97(1), 221-230. <https://doi.org/10.1016/j.neuron.2017.11.020>
- Ioannides, A. A., Corsi-Cabrera, M., Fenwick, P. B., del Rio Portilla, Y., Laskaris, N. A., Khurshudyan, A., ... & Kostopoulos, G. K. (2004). MEG tomography of human cortex and brainstem activity in waking and REM sleep saccades. *Cerebral Cortex*, 14(1), 56-72. <https://doi.org/10.1093/cercor/bhg091>
- Joliot, M., Jobard, G., Naveau, M., Delcroix, N., Petit, L., Zago, L., ... & Tzourio-Mazoyer, N. (2015). AICHA: An atlas of intrinsic connectivity of homotopic areas. *Journal of Neuroscience Methods*, 254, 46-59. <https://doi.org/10.1016/j.jneumeth.2015.07.013>
- Jouvet, M. (1965). Paradoxical sleep—a study of its nature and mechanisms. *Progress in Brain Research*, 18, 20-62.

- Klimesch, W. (1999). EEG alpha and theta oscillations reflect cognitive and memory performance: A review and analysis. *Brain Research Reviews*, 29(2-3), 169-195.
[https://doi.org/10.1016/S0165-0173\(98\)00056-3](https://doi.org/10.1016/S0165-0173(98)00056-3)
- Klinzing, J. G., Niethard, N., & Born, J. (2019). Mechanisms of systems memory consolidation during sleep. *Nature Neuroscience*, 22(10), 1598-1610.
<https://doi.org/10.1038/s41593-019-0467-3>
- Lendner, J. D., Helfrich, R. F., Mander, B. A., Romundstad, L., Lin, J. J., Walker, M. P., ... & Knight, R. T. (2020). An electrophysiological marker of arousal level in humans. *elife*, 9, e55092. <https://doi.org/10.7554/eLife.55092>
- Lenth, R., & Lenth, M. R. (2018). Package ‘lsmeans’. *The American Statistician*, 34(4), 216-221.
- Maquet, P., Laureys, S., Peigneux, P., Fuchs, S., Petiau, C., Phillips, C., ... & Cleeremans, A. (2000). Experience-dependent changes in cerebral activation during human REM sleep. *Nature Neuroscience*, 3(8), 831-836. <https://doi.org/10.1038/77744>
- Maquet, P., Péters, J. M., Aerts, J., Delfiore, G., Degueldre, C., Luxen, A., & Franck, G. (1996). Functional neuroanatomy of human rapid-eye-movement sleep and dreaming. *Nature*, 383(6596), 163-166. <https://doi.org/10.1038/383163a0>
- Maquet, P., Ruby, P., Maudoux, A., Albouy, G., Sterpenich, V., Dang-Vu, T., ... & Laureys, S. (2005). Human cognition during REM sleep and the activity profile within frontal and parietal cortices: a reappraisal of functional neuroimaging data. *Progress in Brain Research*, 150, 219-595. [https://doi.org/10.1016/S0079-6123\(05\)50016-5](https://doi.org/10.1016/S0079-6123(05)50016-5)

Madsen, P. L., Holm, S., Vorstrup, S., Friberg, L., Lassen, N. A., & Wildschjødtz, G. (1991).

Human regional cerebral blood flow during rapid-eye-movement sleep. *Journal of Cerebral Blood Flow & Metabolism*, 11(3), 502-507.

<https://doi.org/10.1038/jcbfm.1991.94>

Maurer, U., Brem, S., Liechti, M., Maurizio, S., Michels, L., & Brandeis, D. (2015). Frontal

midline theta reflects individual task performance in a working memory task. *Brain topography*, 28, 127-134. <https://doi.org/10.1007/s10548-014-0361-y>

Montgomery, S. M., Sirota, A., & Buzsáki, G. (2008). Theta and gamma coordination of

hippocampal networks during waking and rapid eye movement sleep. *Journal of*

Neuroscience, 28(26), 6731-6741. <https://doi.org/10.1523/JNEUROSCI.1227-08.2008>

Nishida, M., Pearsall, J., Buckner, R. L., & Walker, M. P. (2009). REM sleep, prefrontal theta, and the consolidation of human emotional memory. *Cerebral Cortex*, 19(5), 1158-1166.

<https://doi.org/10.1093/cercor/bhn155>

Niso, G., Rogers, C., Moreau, J. T., Chen, L. Y., Madjar, C., Das, S., ... & Baillet, S. (2016).

OMEGA: The open MEG archive. *NeuroImage*, 124, 1182-1187.

<https://doi.org/10.1016/j.neuroimage.2015.04.028>

Nofzinger, E. A., Mintun, M. A., Wiseman, M., Kupfer, D. J., & Moore, R. Y. (1997). Forebrain

activation in REM sleep: an FDG PET study. *Brain Research*, 770(1-2), 192-201.

[https://doi.org/10.1016/S0006-8993\(97\)00807-X](https://doi.org/10.1016/S0006-8993(97)00807-X)

Núñez, A., & Buño, W. (2021). The theta rhythm of the hippocampus: from neuronal and circuit

mechanisms to behavior. *Frontiers in cellular neuroscience*, 15, 649262.

<https://doi.org/10.3389/fncel.2021.649262>

Peigneux, P., Laureys, S., Fuchs, S., Delbeuck, X., Degueldre, C., Aerts, J., ... & Maquet, P.

(2001). Generation of rapid eye movements during paradoxical sleep in humans.

NeuroImage, 14(3), 701-708. <https://doi.org/10.1006/nimg.2001.0874>

Popa, D., Duvarci, S., Popescu, A. T., Léna, C., & Paré, D. (2010). Coherent amygdalocortical

theta promotes fear memory consolidation during paradoxical sleep. *Proceedings of the*

National Academy of Sciences, 107(14), 6516-6519.

<https://doi.org/10.1073/pnas.0913016107>

Rasch, B., & Born, J. (2013). About sleep's role in memory. *Physiological Reviews*.

<https://doi.org/10.1152/physrev.00032.2012>

Rolls, E. T., Huang, C. C., Lin, C. P., Feng, J., & Joliot, M. (2020). Automated anatomical

labelling atlas 3. *NeuroImage*, 206, 116189.

<https://doi.org/10.1016/j.neuroimage.2019.116189>

Scheffzük, C., Kukushka, V. I., Vyssotski, A. L., Draguhn, A., Tort, A. B., & Brankač, J.

(2011). Selective coupling between theta phase and neocortical fast gamma oscillations

during REM-sleep in mice. *PLOS ONE*, 6(12), e28489.

<https://doi.org/10.1371/journal.pone.0028489>

Schielzeth, H., Dingemans, N. J., Nakagawa, S., Westneat, D. F., Allogue, H., Teplitsky, C., ...

& Araya-Ajoy, Y. G. (2020). Robustness of linear mixed-effects models to violations of

distributional assumptions. *Methods in ecology and evolution*, 11(9), 1141-1152.

<https://doi.org/10.1111/2041-210X.13434>

Simor, P., Gombos, F., Szakadát, S., Sándor, P., & Bódizs, R. (2016). EEG spectral power in phasic and tonic REM sleep: Different patterns in young adults and children. *Journal of Sleep Research*, 25(3), 269-277. <https://doi.org/10.1111/jsr.12376>

Simor, P., Szalárdy, O., Gombos, F., Ujma, P. P., Jordán, Z., Halász, L., ... & Bódizs, R. (2021). REM sleep microstates in the human anterior thalamus. *Journal of Neuroscience*, 41(26), 5677-5686. <https://doi.org/10.1523/JNEUROSCI.1899-20.2021>

Simor, P., van der Wijk, G., Nobili, L., & Peigneux, P. (2020). The microstructure of REM sleep: Why phasic and tonic?. *Sleep Medicine Reviews*, 52, 101305. <https://doi.org/10.1016/j.smr.2020.101305>

Tadel, F., Baillet, S., Mosher, J. C., Pantazis, D., & Leahy, R. M. (2011). Brainstorm: A user-friendly application for MEG/EEG analysis. *Computational Intelligence and Neuroscience*, 2011(1), 879716. <https://doi.org/10.1155/2011/879716>

Takahara, M., Kanayama, S., Nittono, H., & Hori, T. (2006). REM sleep EEG pattern: examination by a new EEG scoring system for REM sleep period. *Sleep and Biological Rhythms*, 4, 105-110. <https://doi.org/10.1111/j.1479-8425.2006.00201.x>

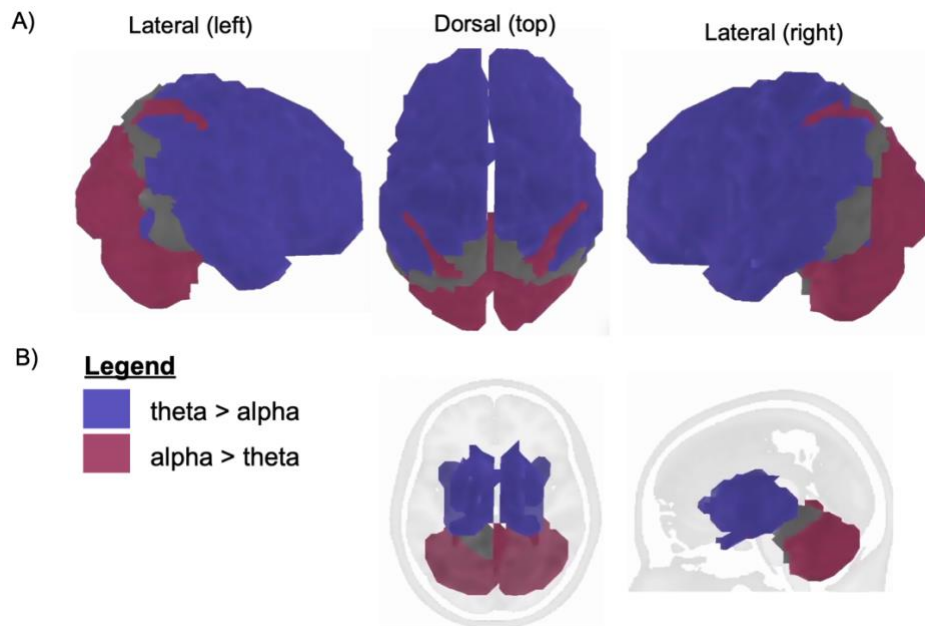
Tamura, M., Spellman, T. J., Rosen, A. M., Gogos, J. A., & Gordon, J. A. (2017). Hippocampal-prefrontal theta-gamma coupling during performance of a spatial working memory task. *Nature communications*, 8(1), 2182. <https://doi.org/10.1038/s41467-017-02108-9>

- Vijayan, S., Lepage, K. Q., Kopell, N. J., & Cash, S. S. (2017). Frontal beta-theta network during REM sleep. *eLife*, 6, e18894. <https://doi.org/10.7554/eLife.18894>
- Wehrle, R., Czisch, M., Kaufmann, C., Wetter, T. C., Holsboer, F., Auer, D. P., & Pollmächer, T. (2005). Rapid eye movement-related brain activation in human sleep: functional magnetic resonance imaging study. *NeuroReport*, 16(8), 853-857.
- Wehrle, R., Kaufmann, C., Wetter, T. C., Holsboer, F., Auer, D. P., Pollmächer, T., & Czisch, M. (2007). Functional microstates within human REM sleep: first evidence from fMRI of a thalamocortical network specific for phasic REM periods. *European Journal of Neuroscience*, 25(3), 863-871. <https://doi.org/10.1111/j.1460-9568.2007.05314.x>
- Wen, H., & Liu, Z. (2016). Separating fractal and oscillatory components in the power spectrum of neurophysiological signals. *Brain Topography*, 29, 13-26. <https://doi.org/10.1007/s10548-015-0448-0>
- Xu, W., De Carvalho, F., Clarke, A. K., & Jackson, A. (2021). Communication from the cerebellum to the neocortex during sleep spindles. *Progress in neurobiology*, 199, 101940. <https://doi.org/10.1016/j.pneurobio.2020.101940>

Supplementary Materials

Appendix A. Characterising REM theta by comparing to alpha (8-12 Hz)

To robustly evaluate differences in theta versus alpha band activity during REM sleep, we conducted LME analysis at the epoch-trial level, using subjects as a random effect. The total number of retained epochs across subjects, after removing outliers and including only values within 1.5 times the IQR from the first and third quartiles, was 2,642,776 (1,321,388 each for theta and alpha). Our analysis identified 276 regions with statistically significant differences in which theta activity was higher than alpha during REM sleep ($p < 0.05$, FDR corrected). Increased activity in the theta band was observed primarily in frontal, central, temporal, and superior parietal regions. Subcortical regions where theta-band activity was significantly greater than alpha-band activity included the hippocampus, medial septum, amygdala, basal ganglia, thalamus, PPN, and LGN. Subsequently, our analysis identified 106 regions with statistically significant differences in which alpha activity was higher than theta during REM sleep ($p < 0.05$, FDR corrected). Alpha activity is predominantly located in occipital regions, including the striate and extrastriate cortices. In addition, the cerebellum, including the vermis, exhibited significantly higher alpha activity compared to theta activity.



Appendix A. Binarized whole-brain spatial topography of statistically significant F-statistic values (derived from LMEs). Purple regions indicate a higher percentage change in oscillatory values over fractal activity within the theta band (5-Hz) compared to the alpha band (8-12 Hz) during REM sleep. Oscillatory activity in the theta band during REM sleep is primarily localised to the frontal, central, temporal, and parietal regions. The hippocampus, medial septum, amygdala, basal ganglia (caudate and putamen), thalamus, PPN, and LGN were identified as subcortical regions where theta-band activity was significantly greater than alpha-band activity. Conversely, pink regions denote a greater percentage change in the alpha band relative to the theta band. Alpha activity is predominantly located in posterior regions of the brain, such as the striate (primary visual cortex), extrastriate cortices, and the cerebellum (including vermis). }

Supplementary Table 1. Maximum and minimum median values during REM sleep within each sliced frequency bin of the 4-8 Hz range (from Figure 1).

Sliced frequency bins	Maximum value	Minimum value
4 Hz	0.55	0.27
5 Hz	0.64	0.22
6 Hz	0.60	0.15
7 Hz	0.62	0.09
8 Hz	0.73	0.39

Supplementary Table 2. Maximum and minimum median values in all sleep stages at 5-7 Hz and during the working memory task (from Figure 4).

Theta 5-7 Hz	Maximum value	Minimum value
Phasic REM sleep	0.62	0.32
Tonic REM sleep	0.70	0.38
S2 K-complex	0.53	0.28
S2 Spindle	0.50	0.26
S2 Plain	0.58	0.23
SWS	0.59	0.27
Working memory	0.65	0.36

Supplementary Table 3. Statistically significant regions of interest showing a higher percent change in oscillatory over fractal activity within the theta band (5-7 Hz) compared to the alpha band (8-12 Hz). The table also indicates regions with a greater percent change in the alpha band relative to the theta band. P-values have been corrected for FDR ($p < 0.05$).

ROI	F-statistic	FDR p-value
G_Angular-1 L	9.25	0.022
G_Angular-1 R	10.75	0.016
G_Angular-3 R	8.27	0.029
G_Cingulum_Ant-1 L	37.01	0.001
G_Cingulum_Ant-1 R	73.94	0.001
G_Cingulum_Ant-2 L	27.68	0.002
G_Cingulum_Ant-2 R	38.70	0.001
G_Cingulum_Mid-1 L	19.00	0.004
G_Cingulum_Mid-1 R	18.69	0.004
G_Cingulum_Mid-2 L	21.68	0.003
G_Cingulum_Mid-2 R	18.08	0.004
G_Cingulum_Mid-3 L	16.28	0.005
G_Cingulum_Mid-3 R	40.13	0.001
G_Cingulum_Post-1 L	14.60	0.007
G_Cingulum_Post-1 R	22.56	0.002

G_Cingulum_Post-2 L	9.49	0.021
G_Cingulum_Post-2 R	10.17	0.018
G_Frontal_Inf_Orb-1 L	77.54	0.001
G_Frontal_Inf_Orb-1 R	25.52	0.002
G_Frontal_Inf_Orb-2 L	21.06	0.003
G_Frontal_Inf_Orb-2 R	14.20	0.007
G_Frontal_Inf_Tri-1 L	43.06	0.001
G_Frontal_Inf_Tri-1 R	35.09	0.001
G_Frontal_Med_Orb-1 L	25.80	0.002
G_Frontal_Med_Orb-1 R	23.05	0.002
G_Frontal_Med_Orb-2 L	27.39	0.002
G_Frontal_Med_Orb-2 R	29.60	0.002
G_Frontal_Mid_Orb-1 L	12.45	0.011
G_Frontal_Mid_Orb-1 R	24.97	0.002
G_Frontal_Mid_Orb-2 L	10.51	0.016
G_Frontal_Mid_Orb-2 R	30.52	0.001
G_Frontal_Mid-1 L	28.16	0.002
G_Frontal_Mid-1 R	29.75	0.001
G_Frontal_Mid-2 L	29.00	0.001
G_Frontal_Mid-2 R	41.89	0.001
G_Frontal_Mid-3 L	29.19	0.001
G_Frontal_Mid-3 R	67.76	0.001
G_Frontal_Mid-4 L	34.37	0.001
G_Frontal_Mid-4 R	49.43	0.001
G_Frontal_Mid-5 L	32.41	0.001
G_Frontal_Mid-5 R	46.88	0.001
G_Frontal_Sup_Medial-1 L	37.51	0.001
G_Frontal_Sup_Medial-1 R	134.59	0.000
G_Frontal_Sup_Medial-2 L	36.32	0.001
G_Frontal_Sup_Medial-2 R	43.43	0.001
G_Frontal_Sup_Medial-3 L	30.03	0.001
G_Frontal_Sup_Medial-3 R	29.65	0.001
G_Frontal_Sup_Orb-1 L	34.56	0.001
G_Frontal_Sup_Orb-1 R	21.56	0.003
G_Frontal_Sup-1 L	33.46	0.001
G_Frontal_Sup-1 R	44.36	0.001
G_Frontal_Sup-2 L	36.85	0.001
G_Frontal_Sup-2 R	36.68	0.001
G_Frontal_Sup-3 L	21.36	0.003
G_Frontal_Sup-3 R	36.47	0.001
G_Fusiform-1 R	7.56	0.034

G_Hippocampus-1 R	19.35	0.003
G_Hippocampus-2 L	6.64	0.044
G_Hippocampus-2 R	11.34	0.014
G_Insula-anterior-1 L	11.01	0.015
G_Insula-anterior-1 R	7.96	0.031
G_Insula-anterior-2 L	28.78	0.002
G_Insula-anterior-2 R	18.09	0.004
G_Insula-anterior-3 L	29.43	0.001
G_Insula-anterior-3 R	42.84	0.001
G_Insula-anterior-4 L	30.69	0.001
G_Insula-anterior-4 R	21.52	0.003
G_Insula-anterior-5 L	21.96	0.003
G_Insula-anterior-5 R	38.67	0.001
G_Insula-posterior-1 L	16.11	0.005
G_Insula-posterior-1 R	25.72	0.002
G_Lingual-1 L	6.50	0.046
G_Paracentral_Lobule-1 L	28.09	0.002
G_Paracentral_Lobule-1 R	31.99	0.001
G_Paracentral_Lobule-2 L	34.31	0.001
G_Paracentral_Lobule-2 R	38.76	0.001
G_Paracentral_Lobule-3 L	30.39	0.001
G_Paracentral_Lobule-3 R	31.83	0.001
G_Paracentral_Lobule-4 L	29.19	0.001
G_Paracentral_Lobule-4 R	33.95	0.001
G_ParaHippocampal-1 L	7.06	0.039
G_ParaHippocampal-1 R	13.74	0.009
G_ParaHippocampal-2 R	7.44	0.035
G_ParaHippocampal-3 L	8.13	0.030
G_ParaHippocampal-3 R	9.34	0.021
G_ParaHippocampal-4 R	11.34	0.014
G_Parietal_Inf-1 L	10.67	0.016
G_Parietal_Inf-1 R	15.40	0.006
G_Parietal_Sup-1 L	16.91	0.005
G_Parietal_Sup-1 R	16.35	0.005
G_Parietal_Sup-2 L	18.85	0.004
G_Parietal_Sup-2 R	17.20	0.005
G_Parietal_Sup-3 L	21.49	0.003
G_Parietal_Sup-3 R	10.74	0.016
G_Parietal_Sup-4 L	10.71	0.016
G_Parietal_Sup-4 R	16.05	0.006
G_Parietal_Sup-5 R	9.12	0.023

G_Precuneus-4 R	8.21	0.030
G_Precuneus-5 R	13.00	0.011
G_Rolandic_Oper-1 L	32.70	0.001
G_Rolandic_Oper-1 R	26.88	0.002
G_Rolandic_Oper-2 L	26.95	0.002
G_Rolandic_Oper-2 R	47.62	0.001
G_subcallosal-1 L	18.16	0.004
G_subcallosal-1 R	22.31	0.002
G_Supp_Motor_Area-1 L	26.58	0.002
G_Supp_Motor_Area-1 R	39.41	0.001
G_Supp_Motor_Area-2 L	28.33	0.002
G_Supp_Motor_Area-2 R	36.74	0.001
G_Supp_Motor_Area-3 L	34.10	0.001
G_Supp_Motor_Area-3 R	30.83	0.001
G_Supramarginal-1 L	21.38	0.003
G_Supramarginal-1 R	37.36	0.001
G_SupraMarginal-2 L	22.76	0.002
G_SupraMarginal-2 R	34.57	0.001
G_Supramarginal-3 L	34.78	0.001
G_Supramarginal-3 R	56.98	0.001
G_Supramarginal-4 L	27.11	0.002
G_Supramarginal-4 R	21.73	0.003
G_SupraMarginal-5 L	19.14	0.004
G_SupraMarginal-5 R	18.57	0.004
G_SupraMarginal-6 L	16.32	0.005
G_SupraMarginal-6 R	13.79	0.008
G_SupraMarginal-7 L	9.87	0.019
G_SupraMarginal-7 R	15.31	0.006
G_Temporal_Inf-1 L	10.53	0.017
G_Temporal_Inf-1 R	16.88	0.006
G_Temporal_Mid-1 L	10.04	0.019
G_Temporal_Mid-1 R	17.54	0.005
G_Temporal_Mid-2 R	6.83	0.042
G_Temporal_Mid-3 L	10.14	0.018
G_Temporal_Mid-3 R	13.27	0.010
G_Temporal_Pole_Mid-1 L	17.57	0.004
G_Temporal_Pole_Mid-2 L	11.98	0.012
G_Temporal_Pole_Mid-3 L	7.76	0.032
G_Temporal_Pole_Mid-3 R	17.58	0.004
G_Temporal_Pole_Sup-1 L	31.59	0.001
G_Temporal_Pole_Sup-1 R	7.74	0.032

G_Temporal_Pole_Sup-2 L	22.74	0.002
G_Temporal_Pole_Sup-2 R	9.56	0.020
G_Temporal_Sup-1 L	26.43	0.002
G_Temporal_Sup-1 R	43.44	0.001
G_Temporal_Sup-2 L	13.73	0.009
G_Temporal_Sup-2 R	25.68	0.002
G_Temporal_Sup-3 L	17.91	0.004
G_Temporal_Sup-3 R	24.95	0.002
G_Temporal_Sup-4 L	16.55	0.005
G_Temporal_Sup-4 R	33.88	0.001
LGNleft	7.53	0.034
LGNright	13.37	0.009
medsep	9.82	0.019
N_Amygdala-1 L	7.25	0.037
N_Amygdala-1 R	9.48	0.020
N_Caudate-1 L	19.85	0.003
N_Caudate-1 R	24.16	0.002
N_Caudate-2 L	27.16	0.002
N_Caudate-2 R	31.97	0.001
N_Caudate-3 L	24.82	0.002
N_Caudate-3 R	21.56	0.002
N_Caudate-4 L	12.51	0.011
N_Caudate-4 R	23.86	0.002
N_Caudate-5 L	13.67	0.009
N_Caudate-5 R	13.79	0.008
N_Caudate-6 L	13.68	0.009
N_Caudate-6 R	19.63	0.003
N_Caudate-7 L	15.85	0.006
N_Caudate-7 R	24.02	0.002
N_Pallidum-1 L	8.21	0.029
N_Pallidum-1 R	18.81	0.004
N_Putamen-2 L	17.99	0.004
N_Putamen-2 R	22.99	0.002
N_Putamen-3 L	9.19	0.022
N_Putamen-3 R	17.50	0.004
N_Thalamus-1 L	7.65	0.033
N_Thalamus-1 R	6.60	0.046
N_Thalamus-2 L	7.78	0.032
N_Thalamus-2 R	10.16	0.018
N_Thalamus-5 R	15.93	0.006
N_Thalamus-6 L	9.55	0.020

N_Thalamus-6 R	10.36	0.017
N_Thalamus-7 R	12.05	0.012
N_Thalamus-8 L	7.19	0.037
N_Thalamus-8 R	9.21	0.022
N_Thalamus-9 R	7.56	0.034
PPNleft	9.40	0.022
PPNright	7.03	0.039
S_Anterior_Rostral-1 L	31.36	0.001
S_Anterior_Rostral-1 R	32.91	0.001
S_Cingulate-1 L	25.64	0.002
S_Cingulate-1 R	27.23	0.002
S_Cingulate-2 L	21.97	0.003
S_Cingulate-2 R	33.00	0.001
S_Cingulate-3 L	27.10	0.002
S_Cingulate-3 R	37.38	0.001
S_Cingulate-4 L	32.71	0.001
S_Cingulate-4 R	36.27	0.001
S_Cingulate-5 L	23.49	0.002
S_Cingulate-5 R	59.60	0.001
S_Cingulate-6 L	23.80	0.002
S_Cingulate-6 R	34.85	0.001
S_Cingulate-7 L	17.58	0.005
S_Cingulate-7 R	25.82	0.002
S_Inf_Frontal-1 L	25.41	0.002
S_Inf_Frontal-1 R	21.28	0.003
S_Inf_Frontal-2 L	49.24	0.001
S_Inf_Frontal-2 R	34.95	0.001
S_Intraparietal-1 L	27.71	0.002
S_Intraparietal-1 R	23.74	0.002
S_Intraparietal-2 R	19.59	0.003
S_Intraparietal-3 R	11.64	0.013
S_Olfactory-1 L	27.07	0.002
S_Olfactory-1 R	21.68	0.003
S_Orbital-1 L	39.14	0.001
S_Orbital-1 R	23.04	0.002
S_Orbital-2 L	37.41	0.001
S_Orbital-2 R	27.47	0.002
S_Postcentral-1 L	26.37	0.002
S_Postcentral-1 R	63.94	0.001
S_Postcentral-2 L	27.69	0.002
S_Postcentral-2 R	31.25	0.001

S_Postcentral-3 L	29.18	0.001
S_Postcentral-3 R	41.04	0.001
S_Precentral-1 L	49.60	0.001
S_Precentral-1 R	79.33	0.001
S_Precentral-2 L	24.35	0.002
S_Precentral-2 R	48.08	0.001
S_Precentral-3 L	32.27	0.001
S_Precentral-3 R	23.63	0.002
S_Precentral-4 L	29.31	0.001
S_Precentral-4 R	33.25	0.001
S_Precentral-5 L	40.16	0.001
S_Precentral-5 R	36.03	0.001
S_Precentral-6 L	25.84	0.002
S_Precentral-6 R	32.10	0.001
S_Rolando-1 L	28.53	0.001
S_Rolando-1 R	57.70	0.001
S_Rolando-2 L	28.82	0.002
S_Rolando-2 R	39.37	0.001
S_Rolando-3 L	21.87	0.003
S_Rolando-3 R	50.13	0.001
S_Rolando-4 L	29.85	0.001
S_Rolando-4 R	41.99	0.001
S_Sup_Frontal-1 L	19.26	0.003
S_Sup_Frontal-1 R	14.23	0.008
S_Sup_Frontal-2 L	22.07	0.002
S_Sup_Frontal-2 R	96.71	0.000
S_Sup_Frontal-3 L	28.57	0.001
S_Sup_Frontal-3 R	67.52	0.001
S_Sup_Frontal-4 L	26.01	0.002
S_Sup_Frontal-4 R	26.88	0.002
S_Sup_Frontal-5 L	18.96	0.004
S_Sup_Frontal-5 R	54.02	0.001
S_Sup_Frontal-6 L	26.63	0.002
S_Sup_Frontal-6 R	37.11	0.001
S_Sup_Temporal-1 L	36.18	0.001
S_Sup_Temporal-1 R	9.78	0.019
S_Sup_Temporal-2 L	12.27	0.012
S_Sup_Temporal-2 R	30.13	0.001
S_Sup_Temporal-3 L	11.62	0.013
S_Sup_Temporal-3 R	20.76	0.003
S_Sup_Temporal-4 L	10.68	0.016

Supplementary Table 4. Statistically significant regions of interest showing greater theta activity during REM sleep compared to NREM sleep, as determined by LME models. P-values have been corrected for FDR ($p < 0.05$).

ROI	F-statistic	FDR p-value
Cerebelum_10_L	25.11	0.013
Cerebelum_10_R	14.04	0.018
Cerebelum_3_L	24.69	0.013
Cerebelum_3_R	13.85	0.018
Cerebelum_4_5_L	23.12	0.013
Cerebelum_4_5_R	17.56	0.014
Cerebelum_6_L	17.91	0.013
Cerebelum_6_R	15.56	0.016
Cerebelum_7b_L	18.19	0.013
Cerebelum_7b_R	17.08	0.015
Cerebelum_8_L	15.64	0.016
Cerebelum_8_R	18.16	0.014
Cerebelum_9_L	13.49	0.018
Cerebelum_9_R	15.74	0.016
Cerebelum_Crus1_L	14.73	0.016
Cerebelum_Crus1_R	14.56	0.018
Cerebelum_Crus2_L	13.53	0.018
Cerebelum_Crus2_R	16.86	0.015
G_Calcarine-1 L	8.33	0.041
G_Calcarine-3 L	7.40	0.049
G_Cingulum_Ant-1 L	14.59	0.016
G_Cingulum_Ant-1 R	13.68	0.018
G_Cingulum_Ant-2 L	18.66	0.013
G_Cingulum_Ant-2 R	15.00	0.016
G_Cingulum_Mid-1 L	7.87	0.043
G_Cingulum_Post-3 R	6.97	0.050
G_Cuneus-1 R	7.78	0.045
G_Cuneus-2 R	7.85	0.046
G_Frontal_Inf_Orb-1 L	12.06	0.022
G_Frontal_Inf_Orb-1 R	11.77	0.021
G_Frontal_Inf_Orb-2 L	25.95	0.013
G_Frontal_Inf_Orb-2 R	11.20	0.026
G_Frontal_Inf_Tri-1 L	25.32	0.010
G_Frontal_Inf_Tri-1 R	7.71	0.046
G_Frontal_Med_Orb-1 L	12.62	0.020
G_Frontal_Med_Orb-1 R	8.03	0.044

G_Frontal_Med_Orb-2 L	28.27	0.013
G_Frontal_Med_Orb-2 R	24.08	0.013
G_Frontal_Mid_Orb-2 L	8.60	0.040
G_Frontal_Sup_Medial-1 L	15.60	0.015
G_Frontal_Sup_Medial-1 R	7.17	0.049
G_Frontal_Sup_Medial-2 L	13.53	0.012
G_Frontal_Sup_Medial-2 R	8.73	0.033
G_Frontal_Sup_Medial-3 L	16.13	0.016
G_Frontal_Sup_Orb-1 L	28.76	0.012
G_Frontal_Sup_Orb-1 R	14.52	0.018
G_Frontal_Sup-1 L	17.19	0.012
G_Frontal_Sup-2 L	19.90	0.013
G_Frontal_Sup-2 R	14.83	0.016
G_Fusiform-1 L	21.42	0.013
G_Fusiform-2 L	20.30	0.013
G_Fusiform-2 R	9.15	0.035
G_Fusiform-3 L	25.35	0.013
G_Fusiform-3 R	9.30	0.035
G_Fusiform-4 L	22.20	0.013
G_Fusiform-4 R	12.18	0.021
G_Fusiform-5 L	29.35	0.010
G_Fusiform-5 R	12.92	0.019
G_Fusiform-6 L	9.91	0.030
G_Fusiform-6 R	10.80	0.026
G_Fusiform-7 L	10.42	0.028
G_Hippocampus-1 L	18.46	0.014
G_Hippocampus-2 L	27.78	0.012
G_Insula-anterior-1 L	23.16	0.013
G_Insula-anterior-2 L	25.70	0.013
G_Insula-anterior-2 R	11.16	0.025
G_Insula-anterior-3 L	14.93	0.016
G_Insula-anterior-3 R	13.60	0.019
G_Insula-anterior-4 L	15.25	0.016
G_Insula-anterior-4 R	10.63	0.027
G_Insula-anterior-5 L	11.55	0.023
G_Lingual-1 L	43.04	0.002
G_Lingual-1 R	10.59	0.027
G_Lingual-2 L	13.09	0.019
G_Lingual-2 R	9.77	0.031
G_Lingual-3 L	10.88	0.026
G_Lingual-3 R	8.54	0.039

G_Lingual-4 L	7.66	0.046
G_Lingual-5 L	8.95	0.037
G_Occipital_Inf-1 L	11.51	0.023
G_Occipital_Inf-1 R	8.91	0.037
G_Occipital_Inf-2 L	14.44	0.016
G_Occipital_Inf-2 R	12.00	0.022
G_Occipital_Lat-1 L	10.70	0.027
G_Occipital_Lat-2 L	10.71	0.027
G_Occipital_Lat-3 R	7.20	0.050
G_Occipital_Lat-4 L	8.42	0.041
G_Occipital_Lat-5 L	9.60	0.032
G_Occipital_Lat-5 R	8.47	0.040
G_Occipital_Mid-1 R	11.67	0.025
G_Occipital_Mid-2 R	7.44	0.048
G_Occipital_Mid-3 R	7.23	0.050
G_Occipital_Pole-1 L	11.77	0.023
G_Occipital_Pole-1 R	9.10	0.035
G_Occipital_Sup-1 R	7.31	0.049
G_Occipital_Sup-2 R	8.80	0.038
G_ParaHippocampal-1 L	20.55	0.013
G_ParaHippocampal-1 R	8.29	0.041
G_ParaHippocampal-2 L	25.97	0.013
G_ParaHippocampal-2 R	8.00	0.045
G_ParaHippocampal-3 L	23.77	0.013
G_ParaHippocampal-3 R	11.97	0.022
G_ParaHippocampal-4 L	24.04	0.013
G_ParaHippocampal-4 R	10.54	0.028
G_ParaHippocampal-5 L	41.72	0.003
G_ParaHippocampal-5 R	8.67	0.039
G_Parietal_Sup-4 L	8.04	0.046
G_Parietal_Sup-5 L	13.07	0.024
G_Precuneus-1 L	7.42	0.049
G_Rolandic_Oper-1 L	18.06	0.013
G_Rolandic_Oper-2 L	10.99	0.019
G_subcallosal-1 L	23.85	0.013
G_subcallosal-1 R	22.24	0.013
G_Temporal_Inf-1 L	25.24	0.013
G_Temporal_Inf-2 L	14.50	0.018
G_Temporal_Inf-3 L	14.91	0.016
G_Temporal_Inf-3 R	7.87	0.045
G_Temporal_Inf-4 L	13.75	0.018

G_Temporal_Inf-4 R	7.82	0.045
G_Temporal_Inf-5 L	10.75	0.027
G_Temporal_Mid-1 L	8.07	0.045
G_Temporal_Mid-2 R	7.64	0.047
G_Temporal_Mid-3 L	12.50	0.023
G_Temporal_Mid-3 R	7.18	0.049
G_Temporal_Pole_Mid-1 L	19.80	0.013
G_Temporal_Pole_Mid-2 L	15.55	0.017
G_Temporal_Pole_Mid-3 L	20.23	0.013
G_Temporal_Pole_Sup-1 L	19.83	0.013
G_Temporal_Pole_Sup-2 L	19.54	0.013
G_Temporal_Sup-1 L	14.57	0.018
G_Temporal_Sup-1 R	8.28	0.042
G_Temporal_Sup-4 L	7.72	0.045
LGNleft	23.70	0.013
medsep	13.55	0.019
N_Amygdala-1 L	22.81	0.013
N_Caudate-1 L	18.10	0.013
N_Caudate-1 R	24.11	0.013
N_Caudate-2 L	18.30	0.013
N_Caudate-2 R	16.40	0.015
N_Caudate-3 L	22.36	0.013
N_Caudate-3 R	17.20	0.015
N_Caudate-4 L	13.89	0.018
N_Caudate-4 R	9.90	0.030
N_Caudate-5 L	16.66	0.015
N_Caudate-5 R	8.68	0.039
N_Caudate-6 L	7.56	0.046
N_Pallidum-1 L	14.28	0.018
N_Putamen-2 L	22.44	0.013
N_Putamen-2 R	7.33	0.049
N_Putamen-3 L	14.33	0.018
N_Thalamus-1 L	12.79	0.020
N_Thalamus-1 R	11.38	0.025
N_Thalamus-2 R	10.83	0.029
N_Thalamus-3 L	11.36	0.025
N_Thalamus-3 R	10.40	0.028
N_Thalamus-4 R	8.20	0.045
N_Thalamus-5 R	8.31	0.045
N_Thalamus-9 L	7.56	0.049
N_Thalamus-9 R	8.48	0.041

PPNleft	19.32	0.013
PPNright	14.23	0.018
S_Anterior_Rostral-1 L	19.08	0.013
S_Anterior_Rostral-1 R	15.67	0.016
S_Cingulate-1 L	16.65	0.015
S_Cingulate-1 R	9.81	0.035
S_Inf_Frontal-2 L	7.94	0.045
S_Intraoccipital-1 L	9.99	0.032
S_Intraoccipital-1 R	15.30	0.019
S_Olfactory-1 L	33.90	0.012
S_Olfactory-1 R	20.79	0.013
S_Orbital-1 L	20.94	0.013
S_Orbital-1 R	11.14	0.026
S_Orbital-2 L	14.89	0.017
S_Orbital-2 R	12.74	0.019
S_Parietooccipital-1 L	13.00	0.019
S_Parietooccipital-2 L	9.31	0.034
S_Parietooccipital-2 R	7.71	0.046
S_Parietooccipital-4 L	12.55	0.020
S_Parietooccipital-5 R	9.74	0.031
S_Postcentral-1 L	10.67	0.021
S_Rolando-2 L	7.83	0.050
S_Sup_Frontal-1 L	12.41	0.020
S_Sup_Frontal-1 R	11.11	0.025
S_Sup_Frontal-2 L	13.62	0.018
S_Sup_Frontal-3 L	12.66	0.019
S_Sup_Frontal-3 R	7.49	0.049
S_Sup_Frontal-4 L	6.94	0.035
S_Sup_Temporal-1 L	19.86	0.013
S_Sup_Temporal-3 L	17.52	0.016
Vermis_1_2	18.17	0.013
Vermis_10	13.34	0.019
Vermis_3	13.44	0.018
Vermis_4_5	9.94	0.029
Vermis_6	13.22	0.019
Vermis_7	16.47	0.015
Vermis_8	17.42	0.015
Vermis_9	16.37	0.015